Environmental Science: Atmospheres

ROYAL SOCIETY OF CHEMISTRY

PAPER

View Article Online
View Journal

Cite this: DOI: 10.1039/d6ea00049e

A study on the nonlinear lag effects of meteorological factors on $PM_{2.5}$ concentrations in Nanjing, China: based on GAM and DLNM models

Yushan Li,[ab] Song Hong,*[ab] Huan Yang,[ab] Qian Wu,[ab] Dan Wang,[ab] Yao Tang,[ab] Zhongyang Wang,[ab] Aiming Liu,[ab] Shengbiao Wu,[c] Bin Chen*[c] and Chao He[d]

Fine particulate matter ($PM_{2.5}$), as the predominant atmospheric pollutant in China, poses a serious threat to public health and socioeconomic development. Meteorological factors play a critical role in shaping its occurrence and evolution. This study analyzes data from Nanjing City between 2015 and 2023, employing trend analysis, Generalized Additive Models (GAM), and Distributed Lag Nonlinear Models (DLNM) to investigate the spatiotemporal distribution of $PM_{2.5}$ and the impact of meteorological variables. The results show that $PM_{2.5}$ concentrations in the city declined overall from 2015 to 2023, at an average rate of −3.36 μg (m^3 per year), exhibiting distinct phased characteristics; $PM_{2.5}$ concentrations were higher in winter than in summer, lower in the central urban area, and higher in industrially developed regions. The GAM model indicates that 2 m temperature (T2M) and boundary layer height (BLH) are the primary driving factors, and the interaction between 2 m temperature–10 m wind speed (T2M–FG10) and BLH–FG10 exerts a strong regulatory effect on pollutant dispersion; when total precipitation (PRE) lies within the range of 0.008–0.013 m and FG10 within the range of 1.0–1.8 m s^{-1}, their interaction has a positive effect on $PM_{2.5}$ concentrations. The results of DLNM show that the lag and cumulative effects of meteorological factors on $PM_{2.5}$ are significant. The lag effect of 0–3 days is the most prominent, and the precipitation removal effect is the strongest in 0–7 days. When T2M increased, the lag effect changed from negative to positive; while BLH increased, the negative lag effect increased. This study reveals the spatiotemporal dynamics of meteorological factors on $PM_{2.5}$ and provides a scientific basis for the precise management of air pollutants in Nanjing.

Received 1st April 2026
Accepted 20th May 2026

DOI: 10.1039/d6ea00049e

rsc.li/esatmospheres

Environmental significance

$PM_{2.5}$ (fine particulate matter) poses severe hazards to environmental systems by reducing air visibility, disrupting climate systems, and driving photochemical reactions for secondary pollutants. Severe global climate change brings about frequent extreme weather and meteorological shifts, raising $PM_{2.5}$ levels by hampering pollutant dispersion. Therefore, further elucidating the influence mechanisms of meteorological elements on $PM_{2.5}$ aids in precise pollution control and long-term regional planning. Most previous studies have focused only on same-day meteorological effects, neglecting the lagged effects of meteorological factors. The lagged effects of meteorology may play a crucial role in the pollution and dispersion processes of $PM_{2.5}$. This paper systematically analyzes the composite lagged mechanisms of regional meteorological factors, providing a scientific basis for refined governance.

1 Introduction

Atmospheric fine particulate matter ($PM_{2.5}$) pollution has become a core issue in global environmental governance due to its multifaceted impacts on human health, ecosystems, and socioeconomic systems. $PM_{2.5}$ (aerodynamic diameter ≤2.5 μm) can enter the human bloodstream *via* the respiratory system, and long-term exposure may induce asthma, cardiovascular diseases, and respiratory disorders.[1–3] According to the World Health Organization (WHO), approximately 7 million premature deaths worldwide in 2012 were attributed to diseases associated with $PM_{2.5}$ exposure.[4] Beyond health risks, $PM_{2.5}$ pollution also causes significant economic losses by reducing air visibility, thereby increasing traffic accidents and flight delays.[5] As a developing country, China is facing severe air pollution challenges in the process of rapid industrialisation. To address this, the State Council successively issued the Air

[a]School of Resource and Environmental Sciences, Wuhan University, Wuhan 430079, China. E-mail: songhongpku@126.com

[b]Key Laboratory of Geographic Information System, Ministry of Education, Wuhan University, Wuhan 430079, China

[c]Future Urbanity & Sustainable Environment (FUSE) Lab, Division of Landscape Architecture, Department of Architecture, Faculty of Architecture, University of Hong Kong, Hong Kong 999077, China. E-mail: binley.chen@hku.hk

[d]National Science Library (Wuhan), Chinese Academy of Sciences, Wuhan 430071, China

Pollution Prevention and Control Action Plan (2013) and the Three-Year Action Plan to Fight Air Pollution (2018), driving the national annual average $PM_{2.5}$ concentration down from 61.8 μg m^{-3} in 2013 to 32.1 μg m^{-3} in 2020.[6] However, regional pollution issues remain unresolved. Take Nanjing as an example: as a major industrial hub in the Yangtze River Delta, its $PM_{2.5}$ concentration decreased from 78 μg m^{-3} in 2013 to 29 μg m^{-3} in 2023. Despite this progress, the city ranked in the lower tier of national air quality indices in 2021.[7] The newly released Implementation Plan for Nanjing's Continuous Air Quality Improvement Action Plan in 2024 further proposes that $PM_{2.5}$ needs to be controlled at 28 μg m^{-3} by 2025, underscoring the urgent need for refined governance measures.[8]

Meteorological factors significantly influence $PM_{2.5}$ concentration dynamics through processes such as diffusion, deposition, and photochemical reactions. Previous studies indicate that conditions of low wind speed (<3.0 m s^{-1}), high humidity (>80%), and low temperature (10–20 °C) tend to promote pollutant accumulation,[9–11] whereas precipitation and strong winds facilitate particulate removal.[12–14] Notably, the influence of meteorological factors on $PM_{2.5}$ often exhibits nonlinear characteristics and lag effects. Numerous scholars have conducted extensive research on the lagged effects of meteorological factors on $PM_{2.5}$ concentrations. For example, Yang *et al.*[15] combined a quantile regression model with a distributed lag nonlinear model (DLNM) to assess the impact of meteorological factors on $PM_{2.5}$ concentrations in 284 Chinese cities between 2015 and 2018, finding that precipitation and wind speed exerted a lag of 2–4 days on $PM_{2.5}$ concentrations. Deng *et al.*[16] analyzed the dynamic relationship between $PM_{2.5}$ pollution and meteorological factors in the Beijing–Tianjin–Hebei region from 2015 to 2020 using the Root-Square-Term (RST) and Panel Vector Autoregression (PVAR) methods and found that meteorological conditions exerted lagged and persistent effects on $PM_{2.5}$ pollution. Duan *et al.*[17] coupled the Distributed Lag Nonlinear Model (DLNM) with the WRF-CMAQ model to assess the impact of meteorological and anthropogenic emission factors on $PM_{2.5}$ concentrations in Handan City, Hebei Province, in 2016 and 2020, and found that meteorological factors exerted a significant non-linear lag effect on $PM_{2.5}$ concentrations. Studies in the Beijing–Tianjin–Hebei region found a 1–3 day delay in $PM_{2.5}$ concentration responses to wind speed and humidity,[18] while research in the Yangtze River Delta region has shown that the promotion of temperature change on the secondary generation of pollutants can last until 48 hours later.[19] Such spatiotemporal heterogeneity underscores the need to develop more precise analytical tools to unravel the complex meteorological–pollution coupling mechanisms.

Current research on the relationship between $PM_{2.5}$ and meteorological factors primarily employs three methodological approaches: (1) spatial regression models (*e.g.*, Geographical and Temporal Weighted Regression, GTWR) can identify regional dominant factors but depend on the assumption of subjective spatial weights;[20] (2) linear regression methods (*e.g.*, Principal Components Regression, PCR) offer high computational efficiency but struggle to capture nonlinear relationships;[21] (3) machine learning models (*e.g.*, Artificial Neural Networks, ANN) offer nonlinear fitting advantages but suffer from interpretability limitations due to their "black box" nature.[22,23] In contrast, Generalized Additive Models (GAM) flexibly characterize nonlinear relationships between variables through smoothing functions and have been successfully applied to investigate $PM_{2.5}$ drivers in the Fenwei Plain.[24] Additionally, the Distributed Lag Nonlinear Model (DLNM) can simultaneously analyze spatiotemporal lag effects in exposure–response relationships and is widely used in epidemiology,[25,26] and it has also been extensively applied in studies of $PM_{2.5}$ in major cities of the Yangtze River Delta. For example, Yang *et al.*[27] used the DLNM model to assess the impact of exposure to air pollutants in Nanjing on precocious puberty; Su *et al.*[28] and Li *et al.*[29] utilized the DLNM model to assess the associations among $PM_{2.5}$, air temperature, and cardiovascular mortality in Shanghai; Lau *et al.*[30] employed the DLNM model to analyze the relationships among influenza, meteorological factors, and $PM_{2.5}$ in Hangzhou; and Jiang *et al.*[31] integrated the DLNM model into an analysis of the association between extreme precipitation and depression in Suzhou. The DLNM model has been extensively applied in the detailed analysis of region-specific mechanisms.

Nanjing is one of the core cities of the Yangtze River Delta, situated in the lower reaches of the Yangtze River. It is characterized as a megacity, an industrial hub, and a transport hub, and its environmental quality has a significant spillover effect on the socio-economic development of the East China region.[32] $PM_{2.5}$ pollution in Nanjing is influenced by both local emissions and regional transport, and the characteristics of atmospheric pollution are constantly evolving in response to factors such as climate change, socio-economic development, and pollution control measures. At the same time, there has been considerable research on $PM_{2.5}$ pollution in Nanjing, including its spatiotemporal evolution patterns and influencing factors. This study conducts a detailed analysis of the regional mechanisms underlying $PM_{2.5}$ responses in Nanjing. This facilitates comparisons with previous findings and helps fill existing research gaps. Furthermore, Nanjing possesses a long-term, continuous environmental monitoring network and has access to comprehensive high-resolution datasets such as ChinaHigh$PM_{2.5}$ and ERA5 reanalysis data, which provide the necessary data support for detailed spatiotemporal analysis. Therefore, this study focuses on Nanjing City, integrating the ChinaHigh$PM_{2.5}$ high-resolution dataset with ERA5 meteorological reanalysis data. Through trend analysis and GAM, it reveals the spatiotemporal evolution patterns and key drivers of $PM_{2.5}$ from 2015 to 2023. Furthermore, a DLNM is constructed to quantify the lag effects and nonlinear impacts of meteorological factors such as temperature, wind speed, and precipitation. The main contributions of this work include: (1) combining GAM and DLNM models and optimizing the lagged cross-term structure to adapt to the meteorological characteristics of Nanjing, we have achieved a more precise analysis of the mechanisms underlying the relationship between meteorological factors and $PM_{2.5}$ concentrations; (2) it provides quantitative evidence for dynamically optimizing pollution warning windows, thereby supporting the achievement of $PM_{2.5}$

control targets outlined in the Implementation Plan for Nanjing's Continuous Air Quality Improvement Action Plan.

2 Materials and methods

2.1 The study area

Nanjing is located in the southwestern part of Jiangsu Province (31°14′N–32°37′N, 118°22′E–119°14′E) (Fig. 1). Positioned at the transition zone between the lower Yangtze River alluvial plain and the southern Anhui hills, it borders Zhenjiang to the east, Anhui Province to the west, the main Yangtze River channel to the north, and the southern Anhui hills to the south. As one of the core cities in the Yangtze River Delta urban cluster, Nanjing covers an area of approximately 6587.04 km^2. The region features a humid subtropical monsoon climate with distinct seasonal variations: short springs and autumns and long winters and summers. The annual average temperature is 15.40 °C, and the area receives abundant rainfall, averaging about 1106 mm annually. However, rainfall distribution is uneven both temporally and spatially, with 62% of annual precipitation occurring between June and August, characterized by a pronounced plum rain season. By the end of 2023, Nanjing's permanent resident population reached 9.55 million, of whom 8.32 million resided in urban areas, achieving an urbanization rate of 87.20%. Accompanying rapid urbanization, the urban heat island effect has intensified, with an annual average temperature difference of 1.80–2.30 °C between the central urban area and suburban regions.[33] Leveraging its unique geographical position, Nanjing has emerged as a key city along the Yangtze River Economic Zone.

2.2 Methods

To investigate the complex non-linear relationship between various meteorological factors and $PM_{2.5}$ in Nanjing from 2015 to 2023, the Generalized Additive Model (GAM) and the

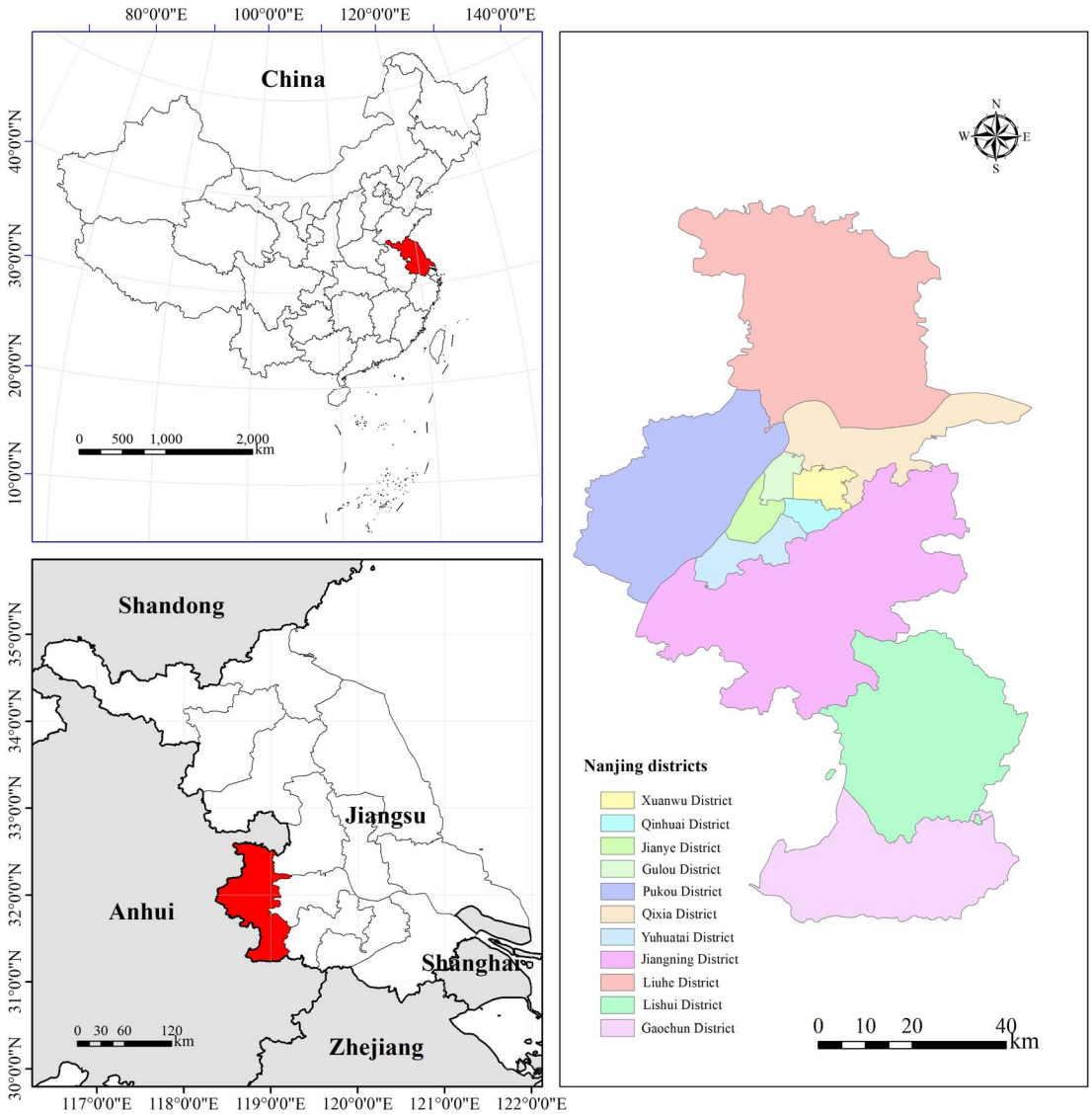

Fig. 1 Overview of Nanjing's geographic location and administrative divisions.

Distributed Lag Nonlinear Model (DLNM) were employed. First, we preprocessed the $PM_{2.5}$ concentration and meteorological data using ArcGIS and Python. We then analyzed the temporal trends of $PM_{2.5}$ and the various meteorological factors using trend analysis methods and mapped the spatial distribution patterns of $PM_{2.5}$ using ArcGIS. Secondly, a GAM model was constructed to analyze the non-linear effects of individual meteorological factors and their interactions on $PM_{2.5}$. Finally, a DLNM model was constructed to identify the lag and cumulative effects of meteorological factors on $PM_{2.5}$. The research framework of this study is illustrated in Fig. 2.

2.2.1 Data sources. The daily $PM_{2.5}$ concentration data from 2015 to 2023 are sourced from the ChinaHigh$PM_{2.5}$ dataset provided by the National Qinghai-Tibet Plateau Science Data Center (https://data.tpdc.ac.cn/), with a daily temporal resolution. Corresponding daily meteorological data were obtained from the ERA5 global reanalysis dataset released by the European Centre for Medium-Range Weather Forecasts (ECMWF: https://cds.climate.copernicus.eu/datasets/derived-era5-single-levels-daily-statistics?tab=overview). Based on previous research[34] and the climatic characteristics of Nanjing, this study selected six indicators, including surface net solar radiation (SSR, J m^{-2}), 2 m temperature (T2M, K), total cloud cover (TCC, dimensionless), total precipitation (PRE, m), 10 m wind speed (FG10, m s^{-1}), and boundary layer height (BLH, m). The primary rationale for this selection is that these variables play a key regulatory role in the formation, transport, and deposition of $PM_{2.5}$. BLH determines the vertical extent of the pollutant mixing zone; a low boundary layer exacerbates near-surface pollution concentrations. T2M regulates pollutant accumulation by influencing atmospheric chemical reaction rates and boundary layer stability. FG10 governs the horizontal dispersion of pollutants. PRE directly removes atmospheric particulate matter through wet deposition. SSR indirectly influences $PM_{2.5}$ concentrations by altering the atmospheric boundary layer and the intensity of photochemical reactions; TCC indirectly influences atmospheric processes by attenuating solar radiation.[33] High-resolution, long-term city-scale data for the selected meteorological factors were obtained from the ERA5 reanalysis, thereby avoiding spatial bias due to sparse monitoring stations; the data cover the period 2015–2023, which is fully aligned with

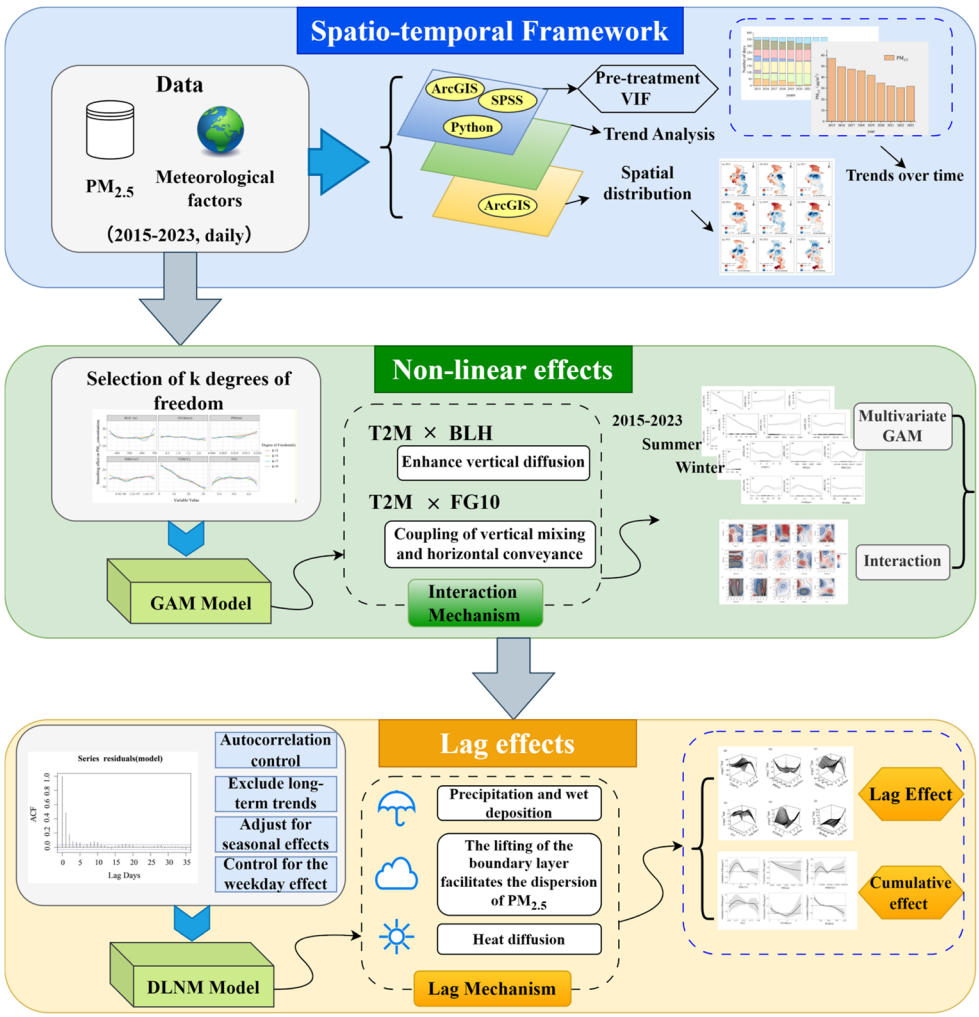

Fig. 2 Research framework used in this study.

the temporal dimension of the $PM_{2.5}$ dataset (ChinaHigh$PM_{2.5}$), ensuring consistency in spatiotemporal analysis. The six selected meteorological factors all have a temporal resolution of daily 24 hour averages for the period 2015–2023, a spatial resolution of 0.25° × 0.25°, and are used to construct the subsequent GAM and DLNM models.

2.2.2 Data preprocessing and collinearity diagnosis. The preprocessing of $PM_{2.5}$ concentration data, including data reading, format conversion, value extraction, and clipping, was completed in ArcGIS 10.8; missing values were removed after extraction. Using Python 3.13.1, the raw meteorological data were read in, missing and outlier values were removed, and panel data on meteorological factors for Nanjing from 2015 to 2023 were compiled. The temperature units were converted to degrees Celsius (°C) using the formula "$T(°C) = T(K) - 273.15$" to facilitate the subsequent construction of the GAM and DLNM models. Before modeling, multicollinearity diagnostics were performed on the variables. The Variance Inflation Factor (VIF) was calculated to detect linear correlations between variables. This study adopts the standard definition and criteria directly, without redefining them. The formula for calculating VIF is as follows:

$$\mathrm{VIF}_i = \frac{1}{1 - R_i^2} \tag{1}$$

In this formula, R_i^2 represents the coefficient of determination obtained from a linear regression of the i-th independent variable against all other independent variables. In this study, VIF values were calculated using the multicollinearity diagnostics function within the "Regression-Linear" module of SPSS Statistics 27. When VIF ≥ 10, strong multicollinearity exists between the variables. The input variables for the multicollinearity diagnosis were the six meteorological factors selected for the study, namely SSR, T2M, TCC, PRE, FG10, and BLH, to test whether there was significant linear correlation between these meteorological factors. If no significant linear multicollinearity is present (*i.e.*, VIF < 10), the interference of linear multicollinearity on model stability can be ruled out, providing an important prerequisite for the subsequent construction of the GAM and DLNM models.

2.2.3 Trend analysis. Trend analysis involves conducting univariate regression on time-series data for variables to reveal patterns of change. This method is commonly used to analyze temporal variations in atmospheric pollutants. It should be noted that this method assumes that the variables exhibit a stationary linear trend over the study period and is used solely to reveal the overall trend of increase or decrease, rather than to provide an accurate description of their variations across the entire time series. The results of the linear trend analysis provide a foundation for subsequent non-linear analyses, facilitating the examination of pollution fluctuation characteristics under different seasonal and meteorological conditions within the overall trend, while the GAM/DLNM models deepen our understanding of the mechanisms underlying these trends.

2015 was a pivotal year for implementing China's Action Plan for the Prevention and Control of Air Pollution (Air Pollution Control Ten Measures); subsequently, Nanjing introduced a series of policies, including the Implementation Plan for the Action Plan on the Continuous Improvement of Air Quality in Nanjing. The period from 2015 to 2023 coincides with the full cycle spanning the conclusion of the Air Pollution Control Ten Measures and the implementation of the 14th Five-Year Plan for Ecological and Environmental Protection, enabling an accurate reflection of the long-term trends in $PM_{2.5}$ concentrations driven by policy and thus holding significant value for policy evaluation. Consequently, this study employs trend analysis to conduct a preliminary quantification of the long-term macro-level trends in $PM_{2.5}$ concentrations in Nanjing from 2015 to 2023, using the following formula:

$$\mathrm{Trend} = \frac{n \times \sum_{i=1}^{n} (i \times \mathrm{PM}_{2.5i}) - \left(\sum_{i=1}^{n} i\right) \times \left(\sum_{i=1}^{n} \mathrm{PM}_{2.5i}\right)}{n \times \sum_{i=1}^{n} i^2 - \left(\sum_{i=1}^{n} i\right)^2} \tag{2}$$

where $PM_{2.5i}$ denotes the $PM_{2.5}$ concentration in year i, n represents the time span, and i indicates the year of observation. First, the annual average $PM_{2.5}$ concentrations are calculated for each year. A simple linear regression is then performed on the annual time series to eliminate the interference of seasonal fluctuations within the year on the trend estimate, thereby obtaining a slope that reflects the long-term trend in $PM_{2.5}$ concentrations. Assuming that the variable exhibits stationary variation, this slope may resemble the rate of change and thus reflect the variable's trend. A positive trend value indicates an increasing trend in $PM_{2.5}$ concentration over time; a negative trend value indicates a decreasing trend; a trend value close to zero suggests minimal variation in $PM_{2.5}$ concentration within the time series, with no significant upward or downward trend, possibly fluctuating around a fixed level.

2.2.4 GAM model. The Generalized Additive Model (GAM) is a semi-parametric extension of the traditional Generalized Linear Model (GLM), designed to analyze nonlinear relationships between a dependent variable and multiple independent variables. It offers greater flexibility by establishing appropriate smoothing functions that automatically select suitable parameters for fitting based on data characteristics, while simultaneously capturing both nonlinear and linear relationships among response variables.[35] GAMs have been extensively applied in fields such as atmospheric pollution and epidemiology. This study constructs a GAM relating $PM_{2.5}$ concentrations to various meteorological factors to analyze their influence on $PM_{2.5}$ levels in Nanjing from 2015 to 2023. After removing outliers and missing values, concentration values were extracted for each grid cell within the Nanjing area and then calculated as monthly averages. Meteorological factor data, including SSR, T2M, TCC, PRE, FG10, and BLH, were resampled to the same spatial resolution as the $PM_{2.5}$ data, and the monthly averages were calculated for each grid cell. The general form of the GAM is as follows:

$$g(\mu) = \beta_0 + f_1(x_1) + f_2(x_2) + \ldots + f_p(x_p) + \varepsilon \tag{3}$$

$$g(\mu) = \mu \tag{4}$$

In eqn (3), μ represents the conditional expected value (*i.e.* the average concentration) of $PM_{2.5}$ under given meteorological conditions; $g(\mu)$ is the link function applied to μ, and in this study a Gaussian distribution is adopted, with the link function given by eqn (4);f_1, f_2,…,f_p are smoothing functions of the independent variables x_1, x_2,…,x_p and represent the nonlinear relationships between the independent variable and the dependent variable. β_0 is the intercept and ε is the error term.

2.2.5 DLNM model. The Distributed Lag Nonlinear Model (DLNM) is employed to describe the association between latent nonlinearity and lagged effects in time series data. The core concept of the DLNM involves using cross-basis functions to model both exposure-response and exposure-lagged effects by selecting appropriate basis functions for each dimension. It simultaneously captures time-lagged effects and nonlinear relationships and finds extensive application in fields such as meteorology and epidemiology. The general form of the DLNM model is as follows:

$$Y_t = \alpha + f(x_t, L) + \varepsilon(t) \quad (5)$$

where x_t denotes the explanatory variable, *i.e.*, the meteorological factors on day t, including SSR, T2M, TCC, PRE, FG10, and BLH. After resampling to the urban scale of Nanjing, the daily mean values of each meteorological factor are calculated and used as the model's explanatory variables; Y_t denotes the response variable, *i.e.* the $PM_{2.5}$ concentration ($\mu g\ m^{-3}$) in Nanjing on day t, after removing outliers and missing values, the $PM_{2.5}$ concentrations at all grid points within the Nanjing area are spatially averaged to obtain the daily mean at the urban scale; $f(x_t, L)$ is a non-linear lag effect function defined by cross-basis functions, used to characterize the cumulative impact of meteorological factors on $PM_{2.5}$ concentrations within the lag period L; L represents the set of discrete points within the lag period range; α is the intercept term; $\varepsilon(t)$ is the error term.

3 Results

3.1 Spatial and temporal distribution of $PM_{2.5}$ concentrations

3.1.1 Temporal changes in $PM_{2.5}$ concentrations. The annual average $PM_{2.5}$ concentration in Nanjing exhibited an overall downward trend from 2015 to 2023 (Fig. S1), indicating a gradual alleviation of $PM_{2.5}$ pollution. The annual average $PM_{2.5}$ concentrations for each year were 57.24 $\mu g\ m^{-3}$, 49.61 $\mu g\ m^{-3}$, 47.43 $\mu g\ m^{-3}$, 45.93 $\mu g\ m^{-3}$, 41.87 $\mu g\ m^{-3}$, 34.76 $\mu g\ m^{-3}$, 32.11 $\mu g\ m^{-3}$, 30.51 $\mu g\ m^{-3}$ and 31.69 $\mu g\ m^{-3}$, all of which exceeded the national limit (25 $\mu g\ m^{-3}$). In terms of the magnitude of change, the largest decrease occurred between 2019 and 2020, amounting to 16.97%, while 2022–2023 showed a slight upward trend, with an increase of 3.84%. Specifically, the overall growth rate of $PM_{2.5}$ concentrations from 2015 to 2023 was −3.36 μg (m^3 per year), indicating a relatively stable, negative downward trend. When analyzed by phase, the growth rate for 2015–2019 (−3.44 μg (m^3 per year)) was negative, indicating a downward trend; the average growth rate for 2020–2023 was 0.60 μg (m^3 per year), with little change during this phase and a slight upward trend. In terms of monthly variations, $PM_{2.5}$ concentrations follow a "U-shaped" distribution, with high levels in winter and spring and low levels in summer and autumn. During winter (December to February), $PM_{2.5}$ concentrations are predominantly concentrated between 60 and 90 $\mu g\ m^{-3}$, representing a period of high incidence of pollution exceeding standards. The proportion of days with $PM_{2.5}$ concentrations exceeding standards reached 51.78% in 2015, stabilizing at below 20% from 2020 onwards. From 2020 onwards, the proportion of days meeting standards in summer reached 100%, while in spring and autumn it stood at over 87% (Fig. 3 and S2).

3.1.2 Spatial variation in $PM_{2.5}$ concentrations. Nanjing's $PM_{2.5}$ concentrations exhibited a spatial pattern characterized

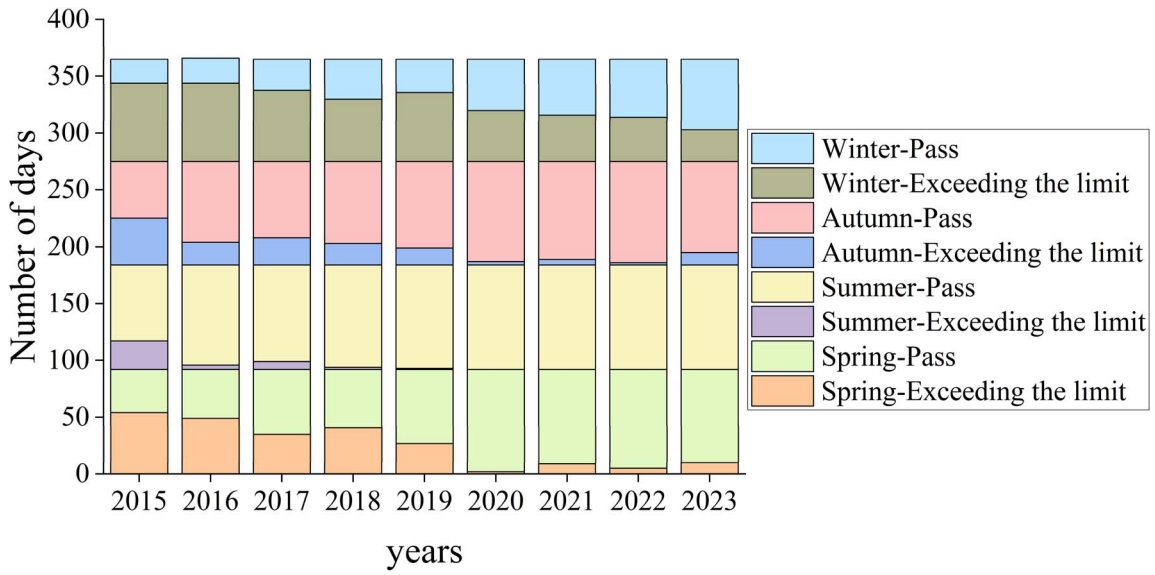

Fig. 3 Number of days with $PM_{2.5}$ concentrations exceeding or meeting standards by season, 2015–2023.

by low-value zones clustering together, while high-value zones were widely distributed between 2015 and 2023 (Fig. 4). Specifically, low-concentration zones were located in eastern Jiangning District in 2015. From 2016 to 2021, they radiated outward from central areas (Jianye District, Gulou District, Xuanwu District, Qinhuai District, western Qixia District, southeastern Pukou District, *etc.*). In 2022 and 2023, they were primarily distributed across central and northern regions. High-value zones were concentrated in the west (Yuhuatai District, Jianye District, western Jiangning District) in 2015, shifted to the north from 2016 to 2020, returned to western Jiangning District in 2021, and concentrated in the southwest (western Gaochun District) and along the Yangtze River in 2022 and 2023. Seasonal variations showed distinct patterns: in 2015, high-value zones exhibited a seasonal distribution pattern of "northwest in spring and summer, southwest in autumn, and central in winter". By 2023, high-value zones across all seasons were predominantly distributed in the south, east, and along the Yangtze River, while low-value zones concentrated in the northern, central, and western regions. Overall, the spatial distribution in 2023 was more dispersed than in 2015 (Fig. S3).

3.2 Nonlinear relationship between meteorological factors and $PM_{2.5}$ concentration

3.2.1 Trends in the temporal variation of various meteorological parameters. Fig. 5 shows the trends in T2M, PRE, SSR, TCC, FG10, and BLH in Nanjing from 2015 to 2023. T2M and BLH generally showed an upward trend, peaking in 2021 and 2022, respectively, before declining; TCC has fluctuated downward since 2020, contrary to the trend observed for SSR; PRE

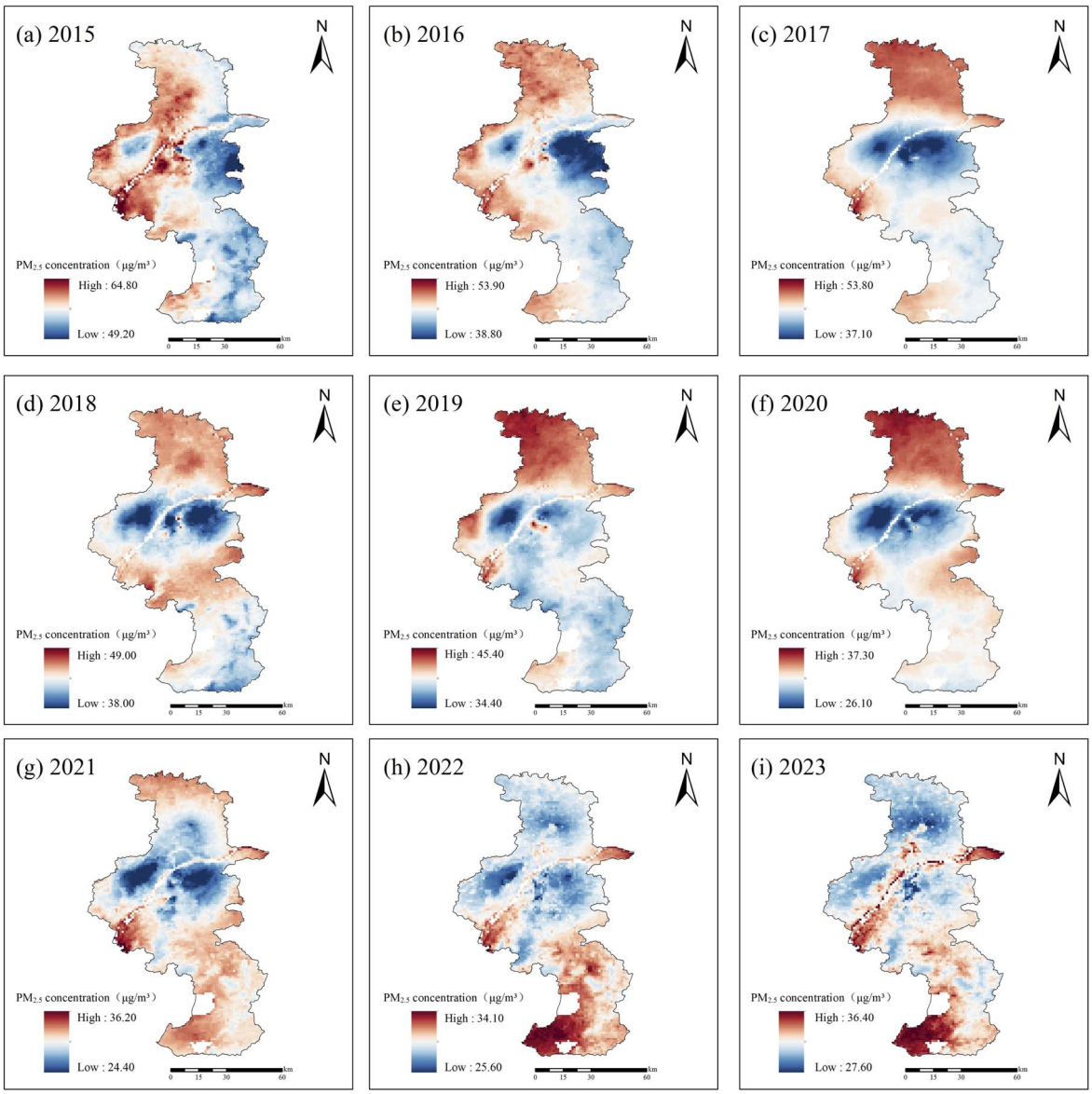

Fig. 4 Spatial distribution of annual average $PM_{2.5}$ concentration in Nanjing, 2015–2023. Note: Panels (a)–(i) sequentially correspond to the annual spatial distribution of $PM_{2.5}$ concentration in Nanjing for 2015, 2016, 2017, 2018, 2019, 2020, 2021, 2022 and 2023, respectively.

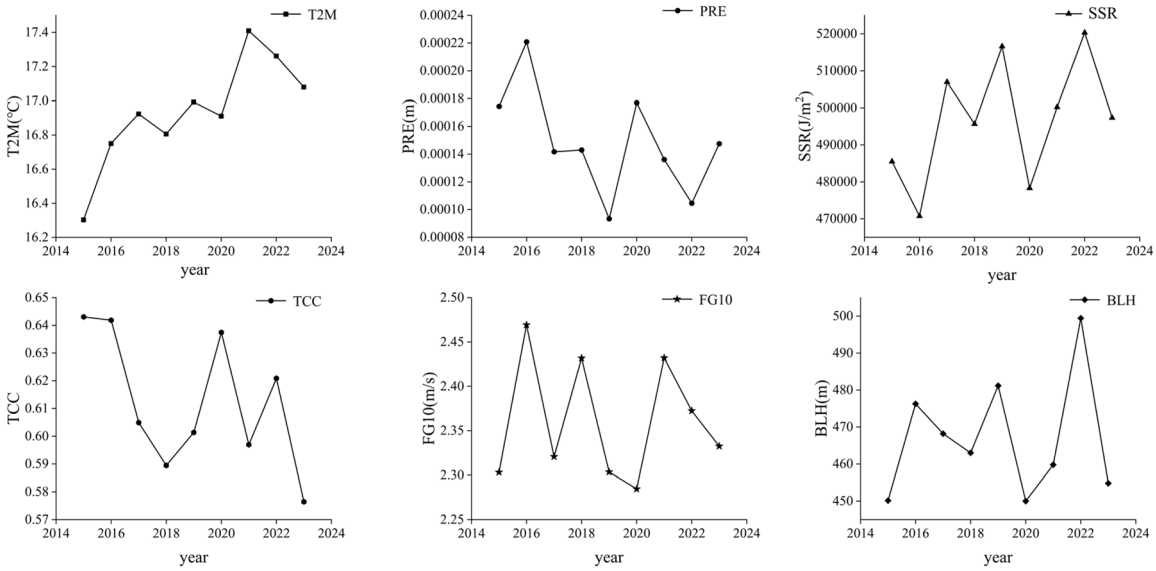

Fig. 5 Trends in various meteorological parameters (T2M, PRE, SSR, TCC, FG10, and BLH) in Nanjing from 2015 to 2023.

and FG10 exhibit significant interannual fluctuations without any clear trend of increase or decrease, being primarily modulated by atmospheric circulation and weather processes. Furthermore, years with high PRE values correspond to years with low SSR and high TCC values, consistent with the principle that cloudy and rainy weather weakens surface radiation. Overall, the core trend in the study area during this period was a warming response in T2M and BLH, while the other variables were characterized primarily by interannual fluctuations; clear physical correlations exist among the variables.

3.2.2 GAM model analysis of $PM_{2.5}$ concentration and multifactor effects. To investigate the impact of meteorological factors on $PM_{2.5}$ concentrations in Nanjing, and in consideration of the city's climatic conditions and existing research,[32] six meteorological parameters (SSR, T2M, TCC, PRE, FG10, and BLH) were chosen as explanatory variables. This study assesses the heterogeneity of the relationship between $PM_{2.5}$ concentrations and meteorological factors from both temporal and seasonal perspectives, analyzing the overall influence patterns of each meteorological factor on $PM_{2.5}$ concentrations across the entire period from 2015 to 2023, as well as the specific characteristics of these influence patterns during the summer and winter seasons of the same period. Calculations using SPSS revealed that the VIF (variance inflation factor) values for all meteorological factors were less than 10 (Table S1), indicating the absence of multicollinearity.

When constructing the GAM model, by setting different degrees of freedom ($k = 3, 5, 7, 9$) for the meteorological factors (T2M, PRE, SSR, TCC, FG10, and BLH) and by comprehensively comparing the model's AIC, explained variance (R^2), effective degrees of freedom (edf) and the shape of the smoothed response curves, a degree of freedom of $k = 5$ was ultimately determined to be the optimal parameter. This setting ensures good non-linear fitting capability while avoiding overfitting or underfitting, and the effect curves are consistent with atmospheric physics (Table S2 and S3 and Fig. S4).

Based on the six selected explanatory variables, a multifactor GAM model of $PM_{2.5}$ in Nanjing was constructed, and a comprehensive analysis covering the entire period from 2015 to 2023 was conducted. The fitting results (Table 1) show that

Table 1 Diagnostic information for the GAM model of $PM_{2.5}$ concentrations and multiple influencing factors in Nanjing, 2015–2023[a]

Years	Smooth term	edf	Ref.df	*F*	*p*-value	Deviance explained	*R*-sq.(adj)
2015–2023	s(T2M)	3.83	3.98	198.34	$<2 \times 10^{-16}$***	72.70%	0.72
	s(PRE)	3.45	3.84	3.89	0.0030**		
	s(SSR)	3.68	3.94	19.34	$<2 \times 10^{-16}$***		
	s(TCC)	3.84	3.98	17.89	$<2 \times 10^{-16}$***		
	s(FG10)	2.27	2.80	7.25	0.0001***		
	s(BLH)	3.92	4.00	18.58	$<2 \times 10^{-16}$***		

[a] edf: effective degrees of freedom, reflecting the degree of non-linear fit of the smoothing terms for each meteorological factor; edf > 1 indicates the presence of a non-linear relationship; Ref.df: reference degrees of freedom, used for the *F*-test and *p*-value calculation; *F*-value: *F*-statistic, measuring the overall significance of the smoothing terms; *p*-value: significance level, $^{**}p < 0.01$, and $^{***}p < 0.001$; deviance explained: proportion of variance explained by the model, reflecting the model's ability to account for variation in $PM_{2.5}$ concentrations; *R*-sq.(adj): adjusted R^2, a modified measure of the model's overall goodness of fit.

the model's coefficient of determination is 72.70% and the adjusted R^2 is 0.72, indicating strong overall explanatory power. The effective degrees of freedom (edf) for all smoothing terms did not exceed the reference degrees of freedom (Ref.df), indicating that the model was not overfitted and the results were reliable. All meteorological factors had a significant impact on $PM_{2.5}$ concentrations, with T2M, SSR, TCC, FG10, and BLH showing $p < 0.001$, and PRE showing $p < 0.01$. The effective degrees of freedom for each meteorological factor were all greater than 1, and the effects were significant ($p < 0.01$), indicating a significant non-linear relationship between $PM_{2.5}$ concentrations and meteorological factors, with the non-linear characteristics of T2M and BLH being particularly pronounced.

Fig. 6, 7, and 8 show the marginal response curves of $PM_{2.5}$ concentrations in Nanjing for the full period, summer, and winter, respectively, in relation to various meteorological factors (T2M, PRE, SSR, TCC, FG10, and BLH) for the years 2015–2023. In the figures, the solid lines represent the marginal effect curves of each meteorological factor on $PM_{2.5}$ concentration, while the dashed lines denote the upper and lower limits of the 95% confidence interval. The effect values were obtained by fitting the smoothing term of the GAM model, with units consistent with $PM_{2.5}$ concentration (μg m^{-3}), reflecting the independent contribution of a single meteorological factor to $PM_{2.5}$. A positive effect value indicates that $PM_{2.5}$ concentrations are higher than the average at that factor level, which tends to promote $PM_{2.5}$ accumulation; a negative effect value indicates that it tends to promote $PM_{2.5}$ removal and reduction. The *x*-axis represents the actual observed values of each variable; the *y*-axis represents the smoothed fitted effect values; and the numbers in brackets denote the effective degrees of freedom, which characterize the degree of non-linearity between the factor and $PM_{2.5}$ concentrations.

The marginal effects and significance of various meteorological factors on $PM_{2.5}$ concentrations in Nanjing are as follows: the marginal response curves for both T2M and FG10 exhibit a monotonically decreasing trend; specifically, for T2M, the effect is positive when the air temperature is below 10 °C, while the negative effect continues to strengthen when the temperature exceeds 20 °C (Fig. 6a). For FG10, the negative effect becomes increasingly pronounced as FG10 increases (Fig. 6e). The marginal effect of SSR exhibits an inverted 'N' shape, with the lowest effect occurring at SSR intensities of 6.0 $\times 10^6$–1.0 $\times 10^7$ J m^{-2} (Fig. 6c). The marginal effect of TCC first rises, then fluctuates steadily, and finally declines. The effect is positive when TCC is approximately 0.5 and decreases significantly when TCC is <0.4 or >0.8 (Fig. 6d). The marginal effect of BLH shows a trend of first declining, then fluctuating steadily, and finally rising, with the effect being lowest at approximately 500 m (Fig. 6f). For PRE levels below 0.010 m, the marginal effect is weak and close to zero, indicating little impact on $PM_{2.5}$. At higher PRE levels (0.010–0.020 m), a slight upward trend is observed, though this trend is based on a small number of observations and thus has high uncertainty, as reflected by the widened confidence intervals (Fig. 6b).

To analyze the heterogeneity in the relationship between $PM_{2.5}$ and meteorological factors at the seasonal level, this study defines June to August as summer and December to

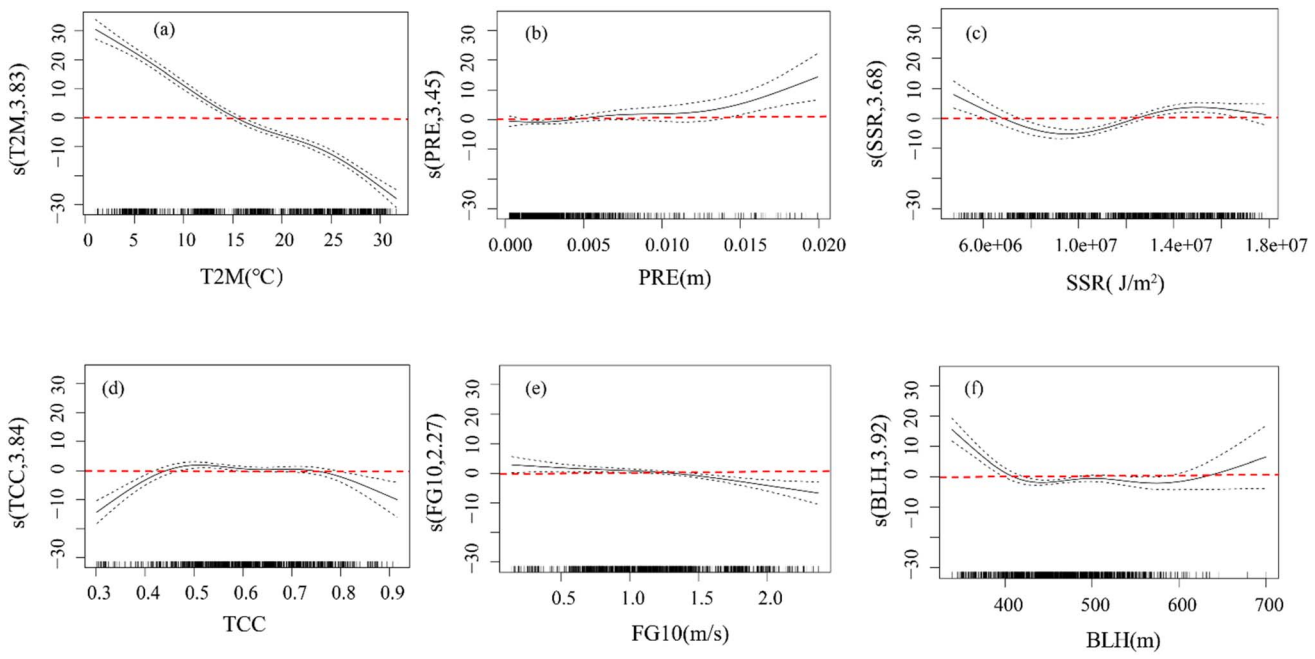

Fig. 6 Response curve of $PM_{2.5}$ concentration to each influencing factor in Nanjing, 2015–2023. Note: Panels (a)–(f) sequentially illustrate the response curves of $PM_{2.5}$ to 2 m temperature (T2M, in °C), total precipitation (PRE, in m), net surface solar radiation (SSR, in J m^{-2}), total cloud cover (TCC, dimensionless), 10 m wind speed (FG10, in m s^{-1}), and boundary layer height (BLH, in m), respectively. The solid lines represent the smoothed fitting curves of the effects of each meteorological factor on $PM_{2.5}$ concentration, reflecting the marginal response trend of $PM_{2.5}$ concentration to changes in that factor when all other factors are held constant at their mean values; the black dotted line indicates the 95% confidence interval, while the red dotted line indicates the $y = 0$ reference line. s() denotes the smoothed fitting term for each factor.

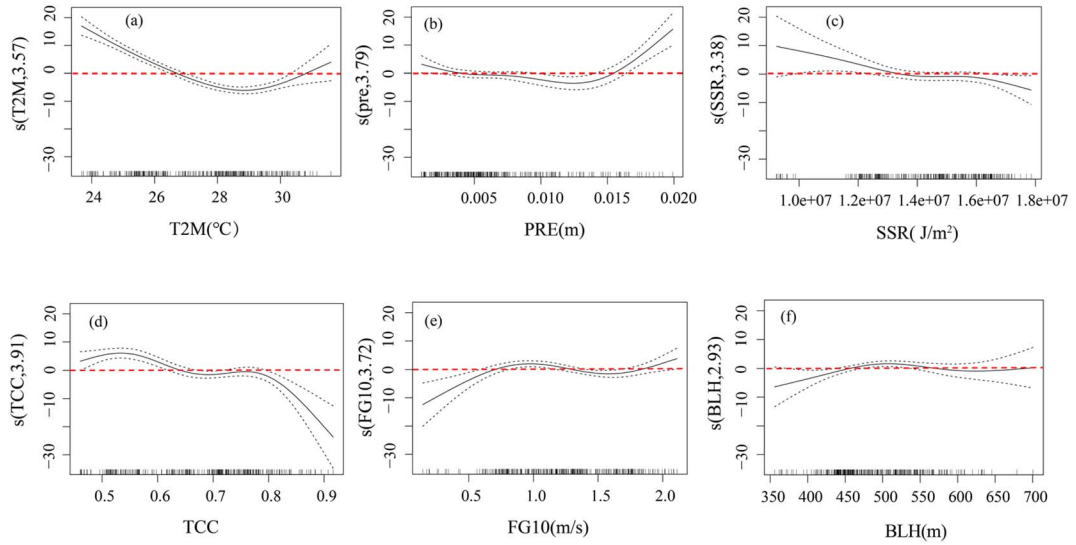

Fig. 7 Response curves of $PM_{2.5}$ concentration to each influencing factor in Nanjing in summer (June, July, and August), 2015–2023. Note: Panels (a)–(f) sequentially illustrate the response curves of $PM_{2.5}$ to 2 m temperature (T2M, in °C), total precipitation (PRE, in m), net surface solar radiation (SSR, in J m^{-2}), total cloud cover (TCC, dimensionless), 10 m wind speed (FG10, in m s^{-1}), and boundary layer height (BLH, in m), respectively. This chart covers the summer months of 2015–2023 in Nanjing, specifically June, July and August. The solid lines represent the smoothed fitting curves of the effects of each meteorological factor on $PM_{2.5}$ concentration, reflecting the marginal response trend of $PM_{2.5}$ concentration to changes in that factor when all other factors are held constant at their mean values; the black dotted line indicates the 95% confidence interval, while the red dotted line indicates the $y = 0$ reference line. s() denotes the smoothed fitting term for each factor.

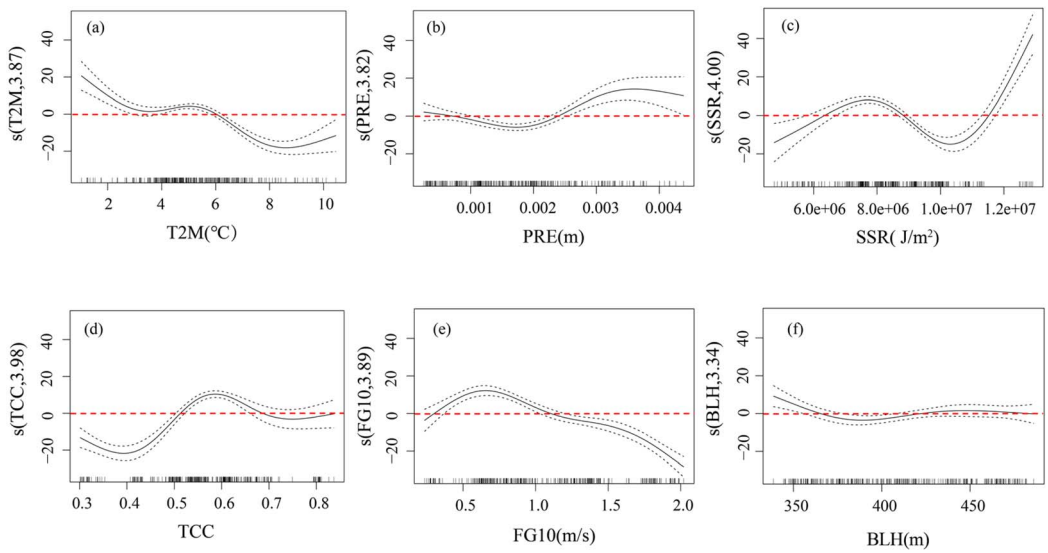

Fig. 8 Response curves of $PM_{2.5}$ concentration to each influencing factor in Nanjing in winter (December, January, and February), 2015–2023. Note: Panels (a)–(f) sequentially illustrate the response curves of $PM_{2.5}$ to 2 m temperature (T2M, in °C), total precipitation (PRE, in m), net surface solar radiation (SSR, in J m^{-2}), total cloud cover (TCC, dimensionless), 10 m wind speed (FG10, in m s^{-1}), and boundary layer height (BLH, in m), respectively. This chart covers the winter months of 2015–2023 in Nanjing, specifically December, January and February. The solid lines represent the smoothed fitting curves of the effects of each meteorological factor on $PM_{2.5}$ concentration, reflecting the marginal response trend of $PM_{2.5}$ concentration to changes in that factor when all other factors are held constant at their mean values; the black dotted line indicates the 95% confidence interval, while the red dotted line indicates the $y = 0$ reference line. s() denotes the smoothed fitting term for each factor.

February as winter and extracts data for these periods from 2015 to 2023 to construct season-specific GAM models (Table 2). The models for summer and winter explained 65.10% and 77.90% of the variance, respectively, with adjusted coefficients of determination of 0.62 and 0.76, indicating strong overall explanatory power. The effective degrees of freedom (edf) for each smoothing term did not exceed the reference degrees of freedom (Ref.df), indicating no overfitting and reliable results. In summer, the effects of T2M, PRE, TCC, and FG10 were highly significant ($p < 0.001$), BLH was significant ($p < 0.05$), and only

Table 2 Diagnostic information for the GAM model of $PM_{2.5}$ influence factors in Nanjing during summer (June, July, and August) and winter (December, January, and February) from 2015 to 2023[a]

	Smooth term	edf	Ref.df	*F*	*p*-value	Deviance explained	*R*-sq.(adj)
Summer	s(T2M)	3.57	3.86	53.95	$<2 \times 10^{-16}$***	65.10%	0.62
	s(PRE)	3.79	3.97	8.50	1.42×10^{-6}***		
	s(SSR)	3.38	3.78	2.23	0.0812		
	s(TCC)	3.91	3.99	13.52	$<2 \times 10^{-16}$***		
	s(FG10)	3.72	3.94	5.75	0.0004***		
	s(BLH)	2.93	3.41	2.41	0.0345*		
Winter	s(T2M)	3.87	3.99	36.05	$<2 \times 10^{-16}$***	77.90%	0.76
	s(PRE)	3.82	3.98	12.16	$<2 \times 10^{-16}$***		
	s(SSR)	4.00	4.00	59.02	$<2 \times 10^{-16}$***		
	s(TCC)	3.98	4.00	41.90	$<2 \times 10^{-16}$***		
	s(FG10)	3.89	3.99	40.21	$<2 \times 10^{-16}$***		
	s(BLH)	3.34	3.78	4.34	0.00198**		

[a] edf: effective degrees of freedom, reflecting the degree of non-linear fit of the smoothing terms for each meteorological factor; edf > 1 indicates the presence of a non-linear relationship; Ref.df: reference degrees of freedom, used for the *F*-test and *p*-value calculation; *F*-value: *F*-statistic, measuring the overall significance of the smoothing terms; *p*-value: significance level, $**p < 0.01$, and $***p < 0.001$; deviance explained: proportion of variance explained by the model, reflecting the model's ability to account for variation in $PM_{2.5}$ concentrations; *R*-sq.(adj): adjusted R^2, a modified measure of the model's overall goodness of fit.

SSR was not significant ($p = 0.0812$). The edf for each significant factor was greater than 1, indicating a significant non-linear relationship between $PM_{2.5}$ and the aforementioned meteorological factors, with PRE and TCC exhibiting more pronounced non-linear characteristics. In winter, all meteorological factors were found to have a significant influence, with T2M, PRE, SSR, TCC and FG10 showing a highly significant effect ($p < 0.001$) and BLH a significant effect ($p < 0.01$); the edf for each factor was greater than 1, indicating a significant non-linear relationship between $PM_{2.5}$ and each meteorological factor, with SSR and TCC exhibiting more pronounced non-linear characteristics.

The marginal responses of $PM_{2.5}$ concentrations in Nanjing during summer and winter from 2015 to 2023 to various meteorological factors exhibited significant seasonal heterogeneity, with T2M and BLH showing the most pronounced seasonal variations. The effect of T2M in summer first decreased and then increased (with a significant negative effect at T2M > 27 °C), while in winter it fluctuated and decreased (with a prominent positive effect at T2M < 4 °C). For BLH, the effect was positive in the altitude range of 450–550 m during summer, while the positive effect was significant in the altitude range less than 380 m during winter. Furthermore, the summer effect of PRE was generally close to 0 (with a significant positive effect only when PRE > 0.015 m). For SSR, the effect during summer was not statistically significant at the conventional level ($p = 0.0812$), whereas the winter effect was significant ($p < 0.001$) and followed a "U-shaped" pattern. For TCC, the summer effect declined, with a positive effect at a range of 0.5–0.6. $PM_{2.5}$ concentrations in summer generally rise initially and then fluctuate slightly as the FG10 increases, whereas in winter they rise initially and then continue to decline as the FG10 increases. Overall, conditions with higher T2M, stronger FG10, and deeper BLH drove $PM_{2.5}$ dispersion in summer, while conditions with lower T2M, shallower BLH, and strong temperature inversions exacerbated pollutant accumulation in winter.

A comparison of the results from the annual and seasonal GAM models reveals that the influence of various meteorological factors on $PM_{2.5}$ exhibits marked seasonal heterogeneity, with some results differing from the overall annual trends. For example, in the annual model, the influence of T2M on $PM_{2.5}$ generally follows a monotonically decreasing trend, whereas the effect curve for T2M in summer exhibits a 'U-shaped' pattern, and in winter, a stronger positive effect is observed in the lower T2M range; SSR exhibits a pronounced inverted 'N-shaped' effect in the annual model, but this effect is not significant in the summer model, showing only a significant 'U-shaped' relationship in winter. Furthermore, the effect of BLH is lowest near 500 m in the annual model, whereas in summer it exhibits a positive effect in the 450–550 m range, and in winter it shows a significant positive effect below 380 m. These differences indicate that the non-linear relationship between meteorological factors and $PM_{2.5}$ is modulated by season. The annual model results represent a composite of seasonal effects, whereas seasonal-specific analyses can more clearly reveal the dominant mechanisms under different meteorological conditions.

3.2.3 Effects of meteorological factor interactions on changes in $PM_{2.5}$ concentrations. This study constructed a two-factor interaction Generalized Additive Model (GAM), generating 15 interaction terms by pairing the six meteorological factors in all possible combinations, to analyze the influence of meteorological factor interactions on $PM_{2.5}$ concentrations in Nanjing between 2015 and 2023. In this model, the 15 interaction terms serve as independent variables and $PM_{2.5}$ concentration as the dependent variable. The fitting results indicate that the model explains 95.50% of the variance, with an adjusted coefficient of determination of 0.95, demonstrating exceptionally strong explanatory power. A statistical significance test for each interaction term (Table 3) reveals that all 15 interaction terms are statistically significant at the $p < 0.001$ level.

Fig. 9 shows a 3D contour plot of the interactive effects of various meteorological factors on $PM_{2.5}$ concentrations. The results of the interaction tests for the GAM model show that all

Table 3 Diagnostic information from the GAM model regarding the interactive effects of various factors on $PM_{2.5}$ concentrations, 2015–2023[a]

Interactive elements	edf	Ref.df	*F*	*p*-value	Deviance explained	*R*-sq.(adj)
te(T2M, FG10)	16.21	24	10.734	$<2 \times 10^{-16}$***	95.50%	0.95
te(T2M, SSR)	7.588	20	5.157	$<2 \times 10^{-16}$***		
te(T2M, PRE)	12.95	20	9.215	$<2 \times 10^{-16}$***		
te(T2M, TCC)	13.587	20	12.381	$<2 \times 10^{-16}$***		
te(T2M, BLH)	15.764	20	7.689	$<2 \times 10^{-16}$***		
te(FG10, SSR)	12.539	16	7.8	$<2 \times 10^{-16}$***		
te(FG10, PRE)	7.936	16	2.726	$<2 \times 10^{-16}$***		
te(FG10, TCC)	7.892	16	3.938	$<2 \times 10^{-16}$***		
te(FG10, BLH)	11.594	16	6.899	$<2 \times 10^{-16}$***		
te(SSR, PRE)	11.71	20	7.72	$<2 \times 10^{-16}$***		
te(SSR, TCC)	16.128	20	11.589	$<2 \times 10^{-16}$***		
te(SSR, BLH)	13.302	19	4.784	$<2 \times 10^{-16}$***		
te(PRE, TCC)	5.678	16	2.203	$<2 \times 10^{-16}$***		
te(PRE, BLH)	10.447	17	6.658	$<2 \times 10^{-16}$***		
te(TCC, BLH)	10.759	17	3.49	$<2 \times 10^{-16}$***		

[a] Interaction term: te(,) denotes the tensor product interaction between two meteorological factors, used to capture the non-linear interaction effect of the combined action of these two factors on $PM_{2.5}$ concentrations; edf: effective degrees of freedom, reflecting the complexity of the non-linear fit for the interaction term; Ref.df: reference degrees of freedom, used for the *F*-test and *p*-value calculation; *F*: *F*-statistic, used to test the overall statistical significance of the interaction term; *p*-value: significance level, where *** indicates $p < 0.001$; deviance explained: proportion of variance explained, reflecting the proportion of $PM_{2.5}$ concentration variation explained by this interaction term alone, demonstrating its independent explanatory power; *R*-sq.(adj): adjusted R^2.

interaction terms passed the significance test ($p < 0.001$), with te(T2M, TCC) having the highest *F*-value (12.381), followed by te(SSR, TCC) (11.589) and te(T2M, FG10) (10.734), while te(PRE, TCC) had the lowest *F*-value (2.203). When T2M < 10 °C and TCC > 0.7, the interaction between the two had a significant positive effect on $PM_{2.5}$ concentration (Fig. 9d); when 1.1×10^7 J m^{-2} < SSR < 1.2×10^7 J m^{-2} and TCC are combined, they exert a positive effect on $PM_{2.5}$ concentration (Fig. 9k); when FG10 <

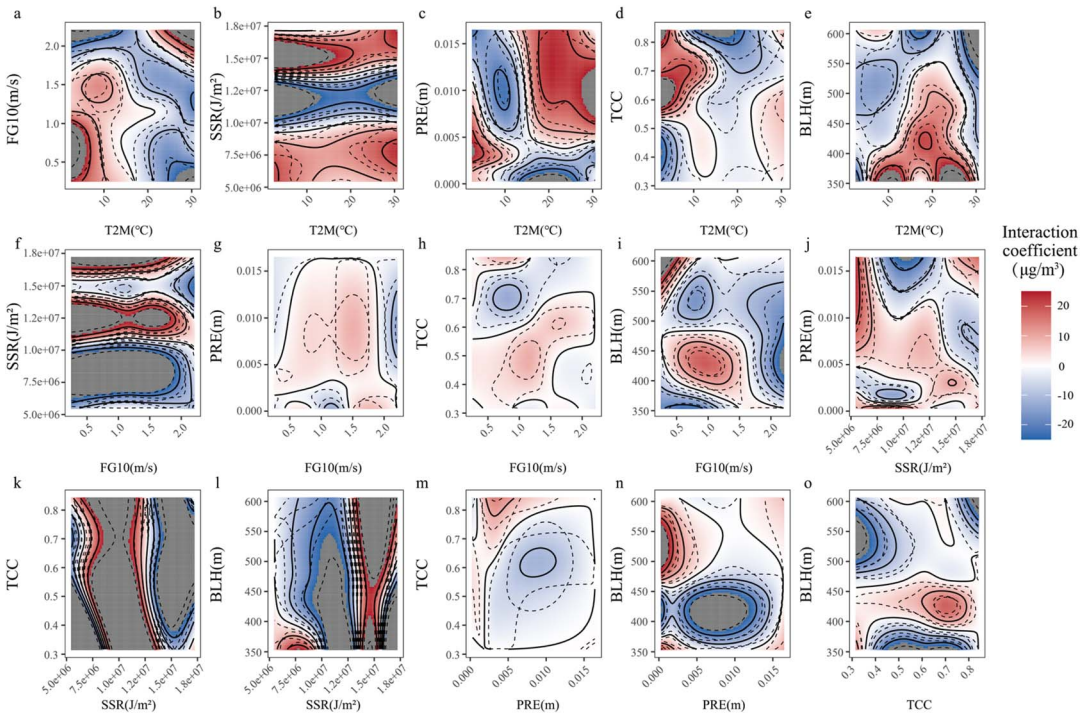

Fig. 9 3D contour map showing the influence of meteorological factor interactions on $PM_{2.5}$ concentrations in Nanjing, 2015–2023. Note: Panels (a)–(o) sequentially illustrate the interaction contours between paired meteorological factors. (a): FG10-T2M; (b): SSR-T2M; (c): PRE-T2M; (d): TCC-T2M; (e): BLH-T2M; (f): SSR-FG10; (g): PRE-FG10; (h): TCC-FG10; (i): BLH-FG10; (j): PRE-SSR; (k): TCC-SSR; (l): BLH-SSR; (m): TCC-PRE; (n): BLH-PRE; (o): BLH-TCC. Solid and dashed contour lines represent interaction effect values (unit: μg m^{-3}); red areas indicate a positive interaction effect (enhancing $PM_{2.5}$ accumulation), while blue areas indicate a negative interaction effect (inhibiting $PM_{2.5}$ accumulation); grey areas indicate regions where the effect is not significant at the 95% confidence level.

1 m s^{-1} and T2M < 5 °C, the interaction between the two has a significant positive effect on $PM_{2.5}$ (Fig. 9a).

Furthermore, the strongest negative effect on $PM_{2.5}$ concentrations occurred under the interaction of 1.0×10^7 J m^{-2}< SSR < 1.3×10^7 J m^{-2} and 5 °C < T2M < 20 °C (Fig. 9b). Significant positive effects were observed for the interaction between PRE near 0.01 m and T2M above 20 °C, and between BLH below 450 m and T2M around 18 °C (Fig. 9c and e). The highest positive effects were found in two interaction combinations: SSR of 1.1×10^7–1.4×10^7 J m^{-2} paired with FG10 of 1.0–2.0 m s^{-1}, and SSR of 1.6×10^7–1.8×10^7 J m^{-2} paired with FG10 of 0.2–1.8 m s^{-1} (Fig. 9f). The strongest positive interaction between PRE and FG10 occurred when PRE was in the range of 0.008–0.013 m and FG10 was in the range of 1.0–1.8 m s^{-1} (Fig. 9g). The positive effect remained consistently high when TCC ranged from 0.3 to 0.7 and FG10 from 0.5 to 1.8 m s^{-1} (Fig. 9h). A positive effect on $PM_{2.5}$ concentration changes was also observed when FG10 was around 1.0 m s^{-1} and BLH was approximately 425 m (Fig. 9i). The weakest negative effects were found in two interaction ranges: PRE of 0.010–0.015 m paired with SSR of 7.5×10^6–1.2×10^7 J m^{-2}, and PRE of 0–0.005 m paired with SSR of 5.0×10^6–1.0×10^7 J m^{-2} (Fig. 9j). Positive effects on $PM_{2.5}$ concentrations were also detected in the interaction ranges of BLH 350–380 m with SSR 5.0×10^6–7.5×10^6 J m^{-2}, and BLH 500–600 m with PRE 0–0.002 m (Fig. 9l and n). A negative effect was observed when PRE ranged from 0.005–0.015 m and TCC from 0.3–0.8 (Fig. 9m), as well as when TCC ranged from 0.3–0.5 and BLH from 500–600 m (Fig. 9o).

3.2.4 Lagged effects of meteorological factors on $PM_{2.5}$ concentrations. To investigate the lag effects of meteorological factors on $PM_{2.5}$ concentrations in Nanjing, this study fitted a DLNM model between $PM_{2.5}$ concentrations and six meteorological parameters (SSR, T2M, TCC, PRE, FG10, and BLH). After removing long-term trends and seasonal fluctuations using natural splines and incorporating month and weekday dummy variables, an ACF test revealed significant short-term autocorrelation in the model residuals and indicated that the time-series autocorrelation had not been fully controlled (Fig. S5). Consequently, an AR (1) structure was applied to correct the model, effectively controlling the autocorrelation. The results of the corrected DLNM model show that the long-term trend term and the month variable controlled by the model were highly significant ($P < 0.001$; $PM_{2.5}$ concentrations exhibited a pattern of being high in winter and spring and low in summer), while the day-of-week effect was only weakly significant for Thursdays ($P < 0.05$). Among the meteorological factors, T2M, PRE, BLH, and FG10 were highly significant for $PM_{2.5}$ concentrations ($P < 0.001$), TCC was weakly significant (P

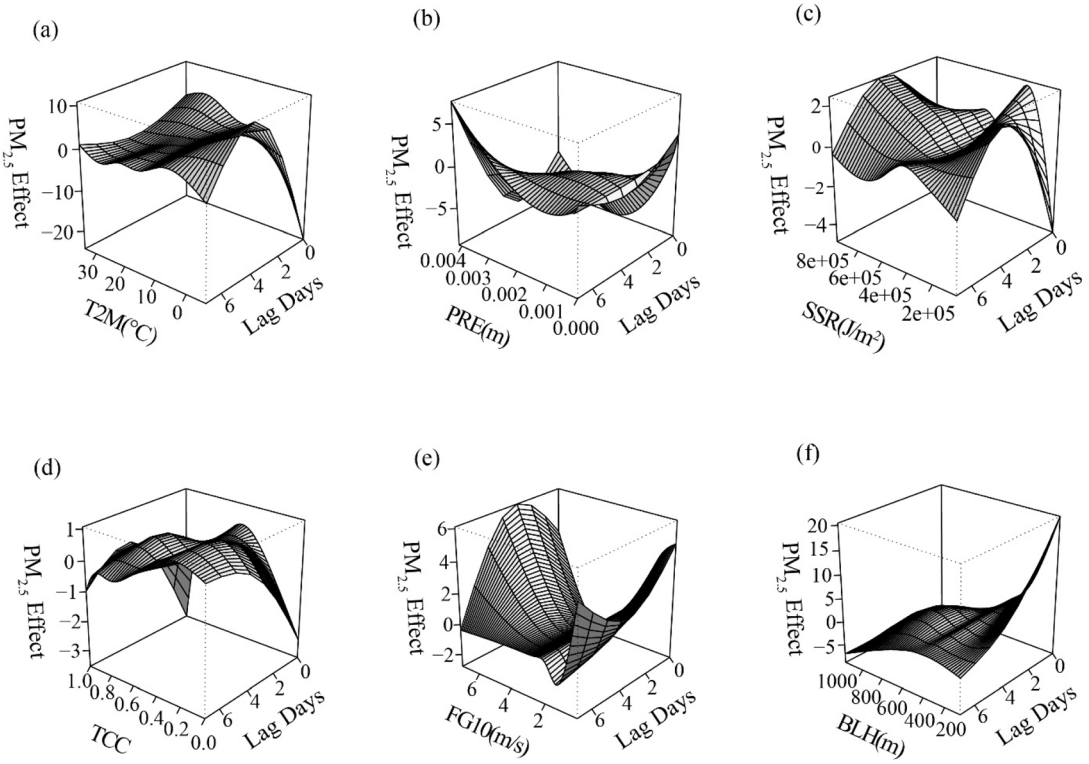

Fig. 10 Response of $PM_{2.5}$ concentrations to each meteorological factor with lags of 0–7 days. Note: Panels (a)–(f) sequentially illustrate the lagged three-dimensional response surfaces of $PM_{2.5}$ for 2 m temperature (T2M, °C), total precipitation (PRE, m), net surface solar radiation (SSR, J m^{-2}), total cloud cover (TCC, dimensionless), 10 m wind speed (FG10, m s^{-1}), and boundary layer height (BLH, m), respectively. Vertical axes denote the marginal effect values of meteorological variables on $PM_{2.5}$ concentration, horizontal axes represent meteorological factor magnitude and lag days.

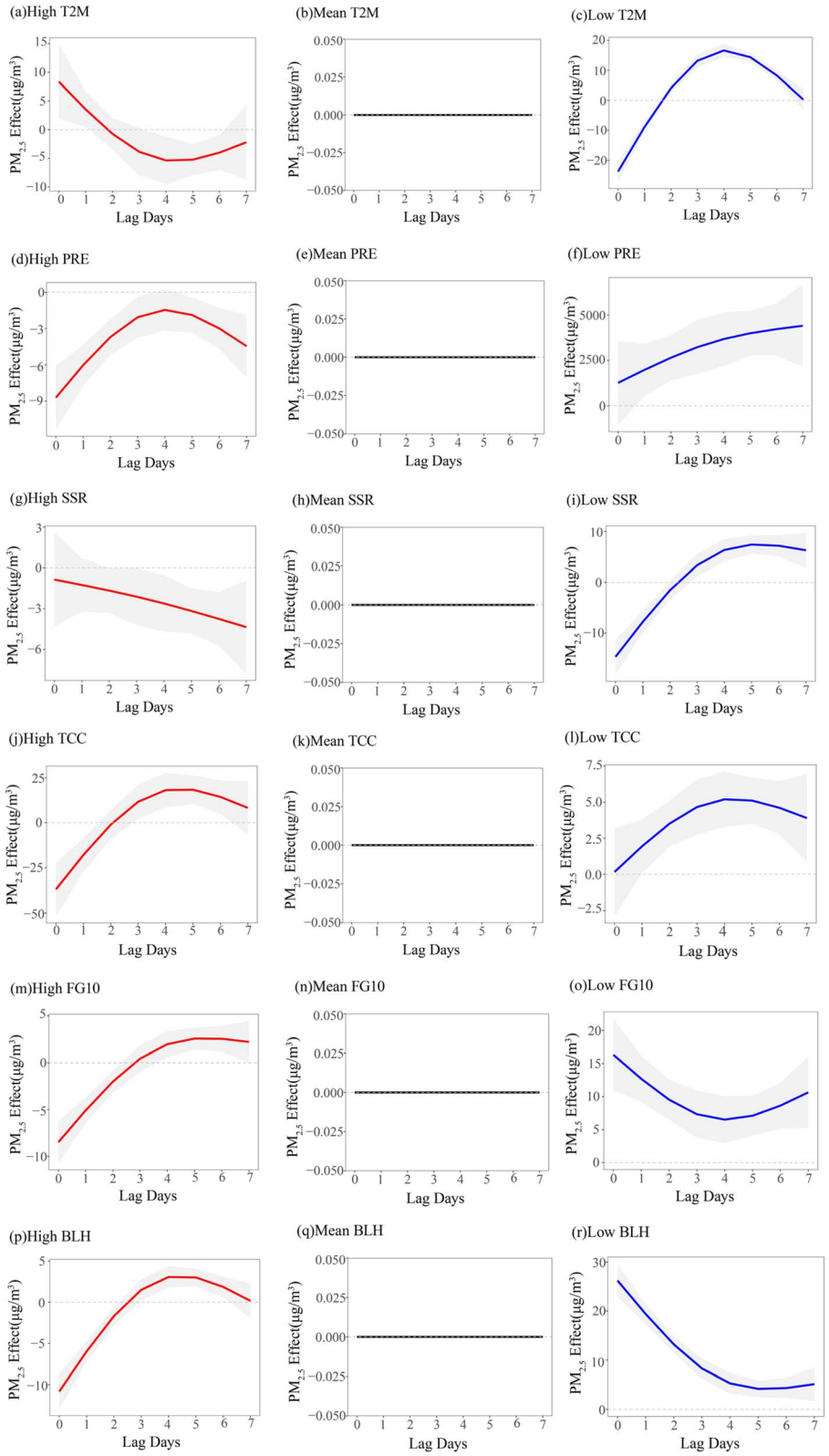

Fig. 11 Lag effect curves for $PM_{2.5}$ concentrations over a 0–7 day period under high, mean, and low values of each influencing factor. Note: Panels (a)–(r) sequentially show lagged $PM_{2.5}$ effects stratified by three levels of meteorological factors. (a–c): High-, mean-, low-level 2 m temperature (T2M, °C); (d–f): High-, mean-, low-level precipitation (PRE, m); (g–i): High-, mean-, low-level net surface solar radiation (SSR, J m^{-2}); (j–l): High-, mean-, low-level total cloud cover (TCC, dimensionless); (m–o): High-, mean-, low-level 10 m wind speed (FG10, m s^{-1}); (p–r): High-, mean-, low-level boundary layer height (BLH, m). Solid lines represent fitted lag effect values, gray shaded areas denote the corresponding 95% confidence intervals, and black dashed lines mark the zero-effect reference line ($y = 0$).

< 0.05), while SSR was not statistically significant ($P > 0.05$) (Table S4).

Fig. 10 illustrates the impact of various factors on $PM_{2.5}$ concentrations, with lags ranging from 0 to 7 days. The *x*-axis represents the values of each influencing factor. The *y*-axis represents the number of lag days. Based on the characteristics of $PM_{2.5}$ and previous research,[36] the maximum lag period in this study was set to 7 days. The *z*-axis represents the magnitude of the effect on $PM_{2.5}$ concentrations. Using the overall daily average of $PM_{2.5}$ in Nanjing during the study period as the reference baseline, the effect value is defined as the deviation of $PM_{2.5}$ concentrations from the average at a specific level of the meteorological factor and a specific lag day, expressed in μg m^{-3}. The number of degrees of freedom for the model variables was selected as 5 based on the Akaike Information Criterion (AIC); the lag periods (0–7 days) were uniformly set to 3 degrees of freedom. This configuration ensures that the lag effect curves are smooth and stable, avoids overfitting, and complies with the construction specifications for non-linear distributed lag models. As shown in Fig. 10, all six meteorological factors exhibit nonlinear lag effects on $PM_{2.5}$. For most factors, the influence is most pronounced within a 0–3 day lag, after which it declines rapidly. Among these, BLH and T2M are the dominant factors influencing $PM_{2.5}$ concentrations. During the lag period, lower T2M had a negative effect on $PM_{2.5}$ concentrations, while higher T2M had a positive effect (Fig. 10a). This change was concentrated within the 0–3 day lag period. As the BLH increased, its effect on $PM_{2.5}$ concentrations showed a decreasing trend (Fig. 10f). When FG10 falls within the range 3 m s^{-1} < FG10 ≤ 5 m s^{-1}, the negative effect on $PM_{2.5}$ is most pronounced during the 0–3 day lag period; when FG10 > 5 m s^{-1}, a negative effect on $PM_{2.5}$ is observed during the 1–3 day lag period (Fig. 10e); furthermore, within a lag of 0–3 days, higher PRE levels exert a negative effect on $PM_{2.5}$ (Fig. 10b), and as TCC increases, a negative effect on $PM_{2.5}$ is observed (Fig. 10d).

To further identify the dynamic relationship between meteorological factors and air pollution, this study plotted lag-effect curves for $PM_{2.5}$ concentrations at low, mean, and high levels of each meteorological factor (Fig. 11; the grey areas represent the 95% confidence intervals). Here, the low value is defined as the mean minus two standard deviations (Low = Mean − 2SD) and the high value as the mean plus two standard deviations (High = Mean + 2SD). The lag effects of all meteorological factors stabilized at 0 at the mean level, and the 95% confidence intervals all included 0, indicating that under average exposure conditions, none of the meteorological factors had a significant lagged effect on $PM_{2.5}$. This result is consistent with the DLNM model's design, which uses the mean as a reference baseline and highlights differences in the effects of extreme exposure levels.

As shown in Fig. 11, the effect of T2M on $PM_{2.5}$ is opposite when T2M is high *versus* low. Over a 1–2 day lag, high T2M exacerbates $PM_{2.5}$ accumulation, whereas low T2M suppresses it. After 2 days, the effects switch to negative and positive, respectively. Both high PRE and high SSR negatively affect $PM_{2.5}$. When FG10 and BLH are high, they both have a negative effect on $PM_{2.5}$ with a lag of 1–3 days; when low, they have a positive effect with a lag of 1–7 days. Low TCC promotes $PM_{2.5}$ accumulation during the lag period.

Fig. 12 illustrates the cumulative effects of various meteorological factors on $PM_{2.5}$ concentrations over a 0–7 day lag, corresponding to the sum of lagged effects across the entire 0–7 day window. The grey areas indicate the 95% confidence intervals. Under conditions where T2M < 16 °C, there is a positive cumulative effect on $PM_{2.5}$ concentrations. PRE and BLH, on the other hand, exhibit a consistently significant negative

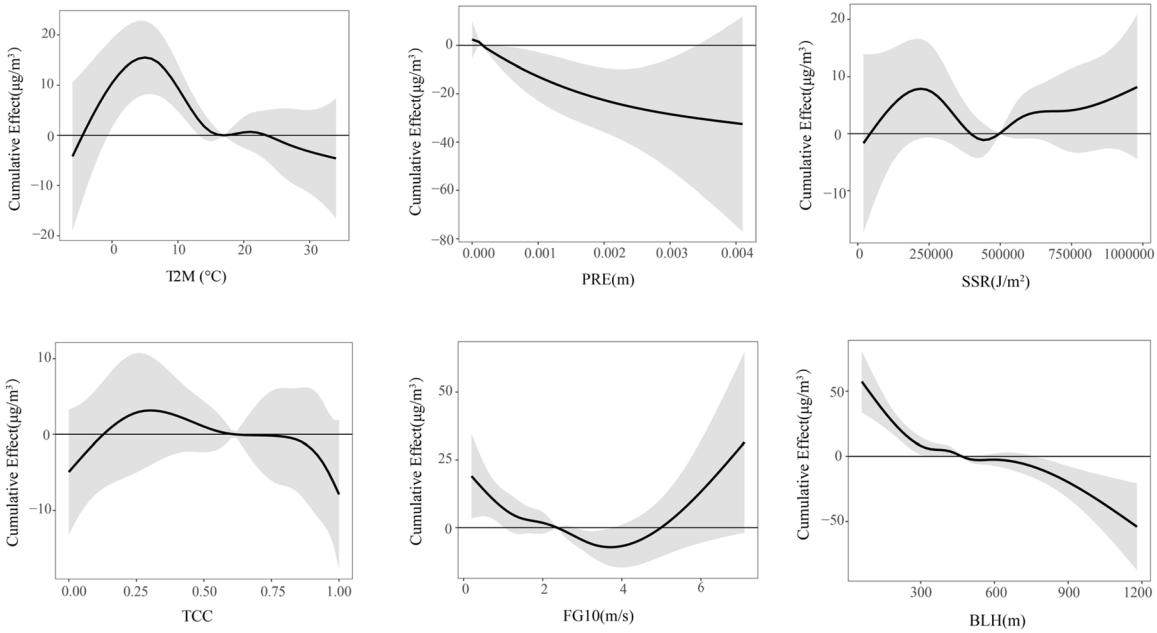

Fig. 12 Cumulative effect curves of $PM_{2.5}$ concentration over a 0–7 day lag time due to each influencing factor.

cumulative effect and are key meteorological factors in clearing $PM_{2.5}$. Furthermore, the confidence intervals for the cumulative effects of the SSR, TCC and FG10 factors largely encompass the zero line, indicating insufficient statistical significance. Among these, only FG10 did not cross the zero line in the confidence interval for the low wind speed range (<2 m s^{-1}); while the local effect is significant, the overall robustness is weak.

4 Discussion

4.1 Spatio-temporal characteristics of $PM_{2.5}$ in Nanjing

The annual average $PM_{2.5}$ concentration in Nanjing decreased significantly from 2015 to 2023, a trend closely linked to the city's ongoing implementation of pollution control policies, including "coal reduction, vehicle emission control, and industrial pollution management". Notably, $PM_{2.5}$ concentrations rose by 3.84% between 2022 and 2023, with an annual average growth rate of 0.60 μg (m^3 per year). This pattern resembles the $PM_{2.5}$ rebound observed in the North China Plain during the same period. The study indicates that meteorological factors are associated with this rebound, accounting for approximately 41% of the impact, with high relative humidity, low wind speeds, and a decrease in atmospheric boundary layer height being the primary driving factors.[37] On a seasonal scale, $PM_{2.5}$ concentrations exhibit a "U"-shaped distribution characterized by "high levels in winter and spring, and low levels in summer and autumn". This is associated with frequent winter temperature inversions,[38] reduced dry deposition due to reduced vegetation,[39] and wet removal by summer precipitation.[40] Spatially, the high-concentration zones of $PM_{2.5}$ in Nanjing shifted from the western industrial belt (Yuhuatai District and western Jiangning District) to spreading southwestward and along the Yangtze River. This change may be linked to the implementation of the "Nanjing Yangtze River Bank Chemical Industry Relocation Plan" in 2017, which led to a 41% decrease in the annual average $PM_{2.5}$ concentration in the western industrial zone by 2021, with high-concentration areas gradually shifting toward Gaochun District in the southwest. Meanwhile, the rise in $PM_{2.5}$ concentrations along the Yangtze River in 2023 may be attributed to ship emissions.[41] The low-concentration zones have shifted from a single cluster in the east to a dispersed pattern spanning the "central urban area and northern Pukou District", a change likely associated with urban greening initiatives and the implementation of traffic restriction policies.

4.2 Mechanisms of the nonlinear effects of meteorological factors on $PM_{2.5}$ concentrations

Results from the GAM model indicate that T2M has a positive effect at temperatures below 10 °C, while the negative effect continues to strengthen at temperatures above 20 °C. This may be related to the fact that, as temperatures rise, photochemical reactions become more active, generating large amounts of VOCs, SO_4^{2-}, and NO_3^-, thereby increasing $PM_{2.5}$ sources.[42] On a seasonal scale, this characteristic shows distinct discrepancies: lower-temperature accumulation dominates in winter and higher-temperature diffusion prevails in summer. However, as temperatures continue to rise, atmospheric convection and vertical diffusion may intensify, thereby reducing near-surface $PM_{2.5}$ concentrations.[43] As FG10 increases, the negative effect on $PM_{2.5}$ gradually strengthens, indicating that wind speed plays a role in pollutant dispersion.[44,45] In contrast to the consistently negative effects observed on an annual scale, seasonal analysis reveals that the dispersive effect of wind speeds during the summer becomes apparent only at higher wind speeds, whereas lower wind speeds in winter are more likely to lead to the accumulation of pollutants. Within the observation area of the study, as the boundary layer height (BLH) gradually increased from approximately 350 m to 500 m, its negative inhibitory effect on $PM_{2.5}$ concentrations gradually intensified. This may be related to the fact that a lower BLH restricts the vertical dispersion of pollutants. From a seasonal perspective, intense solar radiation in summer causes ground-level air to expand as it heats, leading to a significant increase in the atmospheric boundary layer height, which facilitates the upward transport and diffusion of $PM_{2.5}$ near the ground.[34,46] Furthermore, we found that higher PRE values positively affect $PM_{2.5}$. Although precipitation is generally considered one of the most effective mechanisms for removing $PM_{2.5}$ from the atmosphere, it can also lead to high humidity. Under such conditions, $PM_{2.5}$ particles absorb moisture, leading to a significant increase in their size and mass, which in turn elevates the $PM_{2.5}$ mass concentration.[47]

The two-factor interaction in the GAM model reveals complex nonlinear physical mechanisms. When low T2M interacts with low FG10, surface cooling reduces the atmospheric boundary layer height, thereby limiting the dispersion of $PM_{2.5}$. At the same time, low wind speeds hinder the horizontal transport of pollutants; the combined effect of these two factors likely leads to significant accumulation of $PM_{2.5}$ near the ground.[34] When high SSR interacts with high T2M, this combination may significantly promote the conversion of gaseous precursors (such as SO_2, NO_x, and VOCs) into secondary aerosols, thereby exacerbating $PM_{2.5}$ pollution.[48] Furthermore, FG10 and BLH are key meteorological parameters influencing the efficiency of vertical and horizontal pollutant transport. This study found that the interaction of high FG10 and high BLH facilitates $PM_{2.5}$ dispersion, likely because high BLH provides a larger vertical atmospheric space, allowing strong winds to disperse pollutants more easily.[49,50] Moderate PRE interacting with moderate FG10 typically yields the most effective $PM_{2.5}$ removal. This relates to precipitation's ability to remove particulate matter from the atmosphere *via* droplet capture or washout, as well as the role of wind speed in $PM_{2.5}$ removal.[43]

4.3 Mechanisms of atmospheric process responses to lag effects

The lag effects of various meteorological factors on $PM_{2.5}$ concentrations are governed by complex physicochemical mechanisms; understanding these lag mechanisms is crucial for $PM_{2.5}$ forecasting and the formulation of pollution control

strategies. This study indicates that BLH and T2M exert the most pronounced lag effects on $PM_{2.5}$. When the boundary layer height (BLH) is high, the marginal effect on $PM_{2.5}$ is negative within the first 0–3 days of the lag period, and the cumulative effect over the entire lag period is also negative. This may be related to the fact that a high BLH facilitates pollutant dispersion, whereas the diurnal variation in boundary layer height and its impact on vertical mixing and pollutant accumulation typically exhibit a lag of approximately 6–24 hours.[51] High temperatures have a positive effect on $PM_{2.5}$ during the 0–1 day lag period, possibly due to accelerated formation of pollutant precursors. As the lag period extends, precursors are depleted, and thermal convection intensifies; starting from the second day of the lag, the effect turns negative and tends to stabilize, forming a "harvesting effect";[52] low temperatures, on the other hand, may suppress $PM_{2.5}$ formation, and the pattern of their lag effects over time is opposite to that of high temperatures. SSR exhibits a significant negative effect on day 0 of the lag period. Although under high-radiation conditions, precursors such as NO_x generate ozone through photolytic reactions while simultaneously promoting the formation of secondary aerosols (*e.g.*, SO_4^{2-} and NO_3^-), theoretically exhibiting a positive correlation with rising $PM_{2.5}$ concentrations, in Nanjing's summer, high radiation is accompanied by high wind speeds, and diffusion may have a dominant statistical association with decreasing $PM_{2.5}$ concentrations. Conversely, in winter, low radiation is often accompanied by temperature inversions, which are positively correlated with the accumulation of pollutants near the ground. This characteristic reflects the statistical pattern of "dominant factor switching" under multifactorial interactions.[53] Under low-wind conditions, pollutants do not disperse easily, and their effect on $PM_{2.5}$ remains positive over a 0–7 day lag, whereas high FG10 levels exhibit a negative effect on $PM_{2.5}$ over a 1–3 day lag. The mechanism underlying this phenomenon may involve multiple factors, including wind direction and duration. Studies have shown that regional $PM_{2.5}$ transport is a key factor in exacerbating regional pollution, and this transport process itself exhibits significant time lags.[54,55] Precipitation is one of the most effective means of removing atmospheric particulate matter, eliminating $PM_{2.5}$ through wet deposition.[56] As shown in the cumulative effect plots, precipitation plays a significant role in clearing $PM_{2.5}$. However, this study found that when the PRE is low, $PM_{2.5}$ concentrations exhibit a positive effect during the lag period. This may be because trace amounts of precipitation are insufficient for effective wet removal; instead, increased air humidity may promote the hygroscopic growth of particulate matter.[57] When the TCC is high, this may be associated with atmospheric processes that block solar radiation and weaken photochemical reactions, resulting in a cumulative negative effect on $PM_{2.5}$ concentrations over the 0–7 day period. This study utilized the DLNM model to quantify the lag and cumulative effects of meteorological factors in the Nanjing region, addressing the shortcomings of traditional linear models that overlook complex dynamic relationships. It accurately identifies pollution risks during critical periods, providing a scientific basis for formulating refined pollution prevention and control strategies.

4.4 Limitations and future perspectives

This study also has certain limitations. Both meteorological conditions and pollution emissions play significant roles in $PM_{2.5}$ pollution;[58] however, the model used in this study does not currently account for anthropogenic emission factors, which could be incorporated into an anthropogenic emission inventory in future studies. Furthermore, while this study used statistical models to reveal the lag effects and nonlinear relationships between meteorological factors and $PM_{2.5}$ concentrations, it has not yet been able to directly quantify physicochemical mechanisms such as vertical diffusion and regional transport, nor has it conducted a seasonal breakdown and comparison of these lag effects. Future research could be conducted on a larger scale and with greater precision, coupling the "emissions-meteorology" interactions. By comparing and analyzing the influencing factors and lag effects of $PM_{2.5}$ across regions nationwide and globally, relevant theories can be further refined, providing a scientific basis for optimizing air pollution control efforts.

5 Conclusions

This study employs a combined approach of Generalized Additive Models (GAM) and Distributed Lag Nonlinear Models (DLNM) to systematically analyze the spatiotemporal evolution characteristics of $PM_{2.5}$ and its meteorological driving mechanisms in Nanjing from 2015 to 2023. The main conclusions are as follows:

Over time, the annual average concentration of $PM_{2.5}$ in Nanjing has generally declined, though with periodic fluctuations. The growth rate from 2015 to 2019 was -3.44 μg (m^3 per year), and the decline from 2019 to 2020 reached 16.97%. From 2020 to 2023, the average growth rate was 0.60 μg (m^3 per year), with a 3.84% increase from 2022 to 2023. Seasonal variations are significant, with winter concentrations higher than those in summer; in 2015, the proportion of days exceeding standards in winter reached 51.78%. Spatial patterns show that low $PM_{2.5}$ concentration zones are concentrated in the central urban districts (Gulou, Qinhuai, and Xuanwu), while high-concentration zones are distributed in Jiangning and Liuhe, with distinct spatial variations between winter and summer. Analysis of meteorological factors indicates that the marginal response curves for T2M and FG10 both exhibit a monotonically decreasing trend; the marginal effect of SSR generally follows an inverted "N" shape, with the lowest effect occurring at solar radiation intensities of 6.0×10^6–1.0×10^7 J m^{-2}, showing a sustained negative correlation in summer and an "N"-shaped pattern in winter; the marginal effect of BLH first decreases, then fluctuates at a steady level, and finally increases, with the lowest effect at approximately 500 m; the marginal effect of PRE is generally close to 0. The marginal effects of various meteorological factors on $PM_{2.5}$ concentrations in Nanjing during summer and winter from 2015 to 2023 exhibit significant seasonal heterogeneity. Among the interaction effects, the T2M–FG10 combination was the most significant ($F = 10.734$ and edf $= 16.21$). BLH and FG10 were the key meteorological

parameters influencing the vertical and horizontal transport efficiency of pollutants, and the interaction between moderate-intensity PRE and FG10 exerted the most pronounced removal effect.

The lag analysis indicates that meteorological factors have the greatest impact on lags of 0–3 days. High BLH exhibits negative marginal effects on $PM_{2.5}$ within a 0–3 day lag period and negative cumulative effects across the entire lag period. Temperature shifts from a positive to a negative effect at a 2 day lag, with high-PRE and low-PRE exhibiting opposite lag effects. SSR shows a significant negative effect at a 0 day lag, which may be related to the dispersion effect caused by high wind speeds associated with high radiation. Low TCC and low FG10 consistently exhibit positive effects. In terms of cumulative effects, PRE generally has a negative effect. When T2M < 15 °C and FG10 < 2 m s^{-1}, it promotes the accumulation of $PM_{2.5}$. This study reveals the complex nonlinear relationship and lag effects between $PM_{2.5}$ evolution and meteorological conditions, providing a scientific basis for regional air pollution control and prevention.

Author contributions

YL: writing – original draft, writing – review & editing, visualization, validation, methodology, formal analysis, investigation, and conceptualization. SH: writing – review & editing, conceptualization, and methodology. HY: software, visualization, and data curation. QW: investigation and conceptualization. DW: investigation and formal analysis. YT: investigation and validation. ZW: resources and investigation. AL: resources and data curation. SW: writing – review & editing and data curation. BC: writing – review & editing, supervision, and methodology. CH: writing – review & editing, supervision, and conceptualization.

Conflicts of interest

There are no conflicts to declare.

Data availability

Daily $PM_{2.5}$ concentration data from 2015 to 2023 are provided by National Tibetan Plateau/Third Pole Environment Data Center (http://data.tpdc.ac.cn). Corresponding daily meteorological data were obtained from the ERA5 global reanalysis dataset (Copernicus Climate Change Service, Climate Data Store, (2024): ERA5 post-processed daily statistics on single levels from 1940 to present. Copernicus Climate Change Service (C3S) Climate Data Store (CDS), DOI: https://doi.org/10.24381/cds.4991cf48)

Supplementary information (SI): dataset descriptive statistics, multicollinearity diagnosis results (Table S1), GAM optimal smoothing parameter screening results (Tables S2, S3, and Fig. S4), DLNM core regression parameters and residual autocorrelation test outcomes (Table S4 and Fig. S5), meteorological variable definition table (Table S5), and multi-scale temporal-spatial distribution plots of annual/monthly/seasonal $PM_{2.5}$ concentrations (Fig. S1–S3). See DOI: https://doi.org/10.1039/d6ea00049e.

Acknowledgements

The authors would like to express their gratitude to the following scientists for their guidance and assistance in this research: We thank Professors Song Hong and Bin Chen for their guidance on experimental concepts. We acknowledge Huan Yang for providing meteorological data and discussions on data processing. We thank Qian Wu and Dan Wang for discussions on experimental design. We thank Yao Tang and Zhongyang Wang for providing air pollution data. We thank Aiming Liu for discussions on data analysis. We thank Shengbiao Wu for constructive discussions on experimental design. We thank Chao He for guidance on experimental concepts and manuscript writing. We acknowledge Wuhan University, the University of Hong Kong, and the National Science Library (Wuhan) for providing experimental facilities and equipment.

References

1 T. Hou, L. Zhu, Y. Wang and L. Peng, *Food Chem. Toxicol.*, 2024, **184**, 114362.
2 J. Hu, W. Li, Y. Gao, G. Zhao, Y. Jiang, W. Wang, M. Cao, Y. Zhu, Y. Niu, J. Ge and R. Chen, *Environ. Int.*, 2022, **163**, 107218.
3 D. Fang, Q. Wang, H. Li, Y. Yu, Y. Lu and X. Qian, *Sci. Total Environ.*, 2016, **569–570**, 1545–1552.
4 World Health Organization, 2014, https://www.who.int/news/item/25-03-2014-7-million-premature-deaths-annually-linked-to-air-pollution.
5 R. Sawlani, R. Agnihotri and C. Sharma, *Sci. Total Environ.*, 2021, **763**, 142966.
6 X. Niu, Y. Zhong, L. Yang, J. Yi, H. Mu, Q. Wu, S. Hong and C. He, *Environ. Sci.*, 2023, **44**, 1830–1840.
7 Nanjing Municipal People's Government, 2024, https://www.nanjing.gov.cn/njxx/202409/t20240913_4764049.html.
8 Nanjing Municipal People's Government, 2024, https://www.nanjing.gov.cn/zdgk/202408/t20240830_4754281.html.
9 Y. Zu, L. Huang, J. Hu, Z. Zhao, H. Liu, H. Zhang, Q. Ying and M. Chen, *Air Qual. Atmos. Health*, 2017, **10**, 713–724.
10 T. Chen, J. He, X. Lu, J. She and Z. Guan, *Int. Res. J. Publ. Environ. Health*, 2016, **13**, 921.
11 S. Zhou, S. Peng, M. Wang, A. Shen and Z. Liu, *Atmosphere*, 2018, **9**, 343.
12 Q. Yang, Q. Yuan, T. Li, H. Shen and L. Zhang, *Int. Res. J. Publ. Environ. Health*, 2017, **14**, 1510.
13 J. Shen, N. Cao and Y. Zhao, *Clean:Soil, Air, Water*, 2023, **51**, 2100391.
14 L. Wang, K. Qin and B. Zhao, *Atmos. Environ.*, 2024, **329**, 120534.
15 Z. Yang, J. Yang, M. Li, J. Chen and C. Ou, *J. Clean. Prod.*, 2021, **278**, 123931.
16 C. Deng, C. Qin, Z. Li and K. Li, *Chemosphere*, 2022, **301**, 134640.

17 W. Duan, X. Wang, S. Cheng, R. Wang and J. Zhu, *Environ. Pollut.*, 2021, **285**, 117512.
18 P. Wang, H. Guo, J. Hu, S. H. Kota, Q. Ying and H. Zhang, *Sci. Total Environ.*, 2019, **662**, 297–306.
19 Z. Wang, R. Cao, B. Li, M. Cai, Z. Peng, G. Zhang, Q. Lu, H. He, J. Zhang, K. Shi, Y. Liu, H. Zhang and X. Hu, *Environ. Res.*, 2023, **236**, 116854.
20 L. Yang, C. Qin, K. Li, C. Deng and Y. Liu, *Int. Res. J. Publ. Environ. Health*, 2023, **20**, 1183.
21 D. Han, M. Wang, T. Zhang, X. Zhang, J. Liu and Y. Tan, *Urban Clim.*, 2024, **58**, 102160.
22 S. Gao, X. Cheng, J. Yu, L. Chen, Y. Sun, Z. Bai, H. Xu, M. Azzi and H. Zhao, *Atmos. Pollut. Res.*, 2023, **14**, 101905.
23 J. Ma, S. Wan, S. Xu, C. Wang and D. Qiu, *J. Meteorol. Res.*, 2024, **38**, 249–261.
24 H. Li, H. Su, T. Zhang, Z. Zhao and L. Wang, *Environ. Chem.*, 2024, **43**, 1585–1598.
25 M. Quijal-Zamorano, M. Martinez-Beneito, J. Ballester and M. Marí-Dell'Olmo, *Int. J. Epidemiol.*, 2024, **53**, dyae061.
26 A. Sharma, H. Hsiao, J. Liu, S. Lung, H. Su, C. Shen, N. Chen, P. Wu, C. Lin, S. Liang, T. Cheng, T. Chan, Y. Tsay, H. Chung and Y. Wang, *Air Qual. Atmos. Health*, 2024, **17**, 1535–1545.
27 H. Yang, A. Ge, H. Xie, W. Li, Y. Qin, W. Yang, D. Wang, W. Gu and X. Wang, *J. Clin. Med.*, 2022, **12**, 282.
28 W. Su, H. Liu, T. Han, Y. Wang, Y. An and Y. Lin, *BMC Public Health*, 2024, **24**, 3621.
29 Q. Li, S. Li, T. Zhai, S. Jin, C. Wang, B. Fang and T. Xia, *Atmosphere*, 2025, **16**, 119.
30 S. Lau, W. Cheng, Z. Yu, K. Mohammad, M. Wang, B. Zee, X. Li, K. Chong and E. Chen, *Influenza Other Respir. Viruses*, 2021, **15**, 513–520.
31 G. Jiang, Y. Ji, C. Chen, X. Wang, T. Ye, Y. Ling and H. Wang, *BMC Public Health*, 2022, **22**, 1710.
32 T. Tan, X. Xu, H. Gu, L. Cao, T. Liu, Y. Zhang, J. Wang, M. Chen, H. Li and X. Ge, *Toxics*, 2024, **12**, 868.
33 D. Zhang, T. Shen, D. Wang and M. Wang, *Meteorol. Hydrol. Mar. Instrum.*, 2024, **41**, 67–69.
34 Z. Chen, D. Chen, C. Zhao, M. Kwan, J. Cai, Y. Zhuang, B. Zhao, X. Wang, B. Chen, J. Yang, R. Li, B. He, B. Gao, K. Wang and B. Xu, *Environ. Int.*, 2020, **139**, 105558.
35 T. Ouarda, C. Charron, Y. Hundecha, A. St-Hilaire and F. Chebana, *Environ. Model. Software*, 2018, **109**, 256–271.
36 Z. Yang, J. Yang, M. Li, J. Chen and C. Ou, *J. Clean. Prod.*, 2021, **278**, 123931.
37 Q. Song, L. Huang, Y. Zhang, Z. Li, S. Wang, B. Zhao, D. Yin, M. Ma, S. Li, B. Liu, L. Zhu, X. Chang, D. Gao, Y. Jiang, Z. Dong, H. Shi and J. Hao, *Environ. Sci. Technol. Lett.*, 2025, **12**, 305–312.
38 Y. Li, M. Liu, C. Guan and J. Shi, *Acta Sci. Circumst*, 2025, **45**, 1–12.
39 L. Zhang, J. He, S. Gong, X. Guo, T. Zhao, C. Zhou, H. Wang, J. Mo, K. Gui, Y. Zheng, Y. Shan, J. Zhong, L. Li, Y. Lei and H. Che, *Sci. Total Environ.*, 2022, **828**, 154211.
40 D. Lv, Y. Chen, T. Zhu, T. Li, F. Shen, X. Li and T. Mehmood, *Atmos. Pollut. Res.*, 2019, **10**, 1159–1164.
41 X. Zhang, R. Van Der A, J. Ding, X. Zhang and Y. Yin, *Atmos. Chem. Phys.*, 2023, **23**, 5587–5604.
42 S. Zhang, L. Han, W. Zhou and X. Zheng, *Acta Ecol. Sin.*, 2016, **36**, 7897–7907.
43 T. Wang, H. Song, F. Wang, S. Zhai, Z. Han, D. Wang, X. Li, H. Zhao, R. Ma and G. Zhang, *J. Clean. Prod.*, 2020, **274**, 122926.
44 M. Guo, L. Han, X. Huang and B. Li, *Trans. Atmos. Sci.*, 2024, **47**, 809–825.
45 Y. Zhang, J. Sui, X. Wu, M. Lin, L. Chen and T. Chen, *Acta Ecol. Sin.*, 2021, **41**, 2272–2281.
46 J. Ni, Y. Zhao, B. Li, J. Liu, Y. Zhou, P. Zhang, J. Shao, Y. Chen, J. Jin and C. He, *Atmos. Pollut. Res.*, 2023, **14**, 101932.
47 B. Foy and J. Schauer, *Atmos. Res.*, 2024, **307**, 107500.
48 Z. Gao, C. Ivey, C. Blanchard, K. Do, S. Lee and A. Russell, *Sci. Total Environ.*, 2023, **891**, 164464.
49 B. Cheng, Y. Ma, Y. Zhao, P. Qin, F. Feng, Z. Liu, W. Wang and Y. Zhang, *Sci. Total Environ.*, 2024, **934**, 173362.
50 O. Salehie, M. Jamal and S. Shahid, *Theor. Appl. Climatol.*, 2024, **155**, 9081–9097.
51 M. Lu, S. Han, X. Tang, X. Chen, K. Liu, J. Ding, T. Hao and Z. Wang, *Atmos. Res.*, 2025, **315**, 107843.
52 J. Schwartz, *Epi*, 2001, **12**, 55–61.
53 Q. Li, H. Zhang, X. Jin, X. Cai and Y. Song, *Sci. Total Environ.*, 2022, **806**, 150625.
54 Y. Wu, H. Lin, C. Zeng, S. Cao and F. Wei, *Environ. Monit. Forewarn.*, 2024, **16**, 86–90.
55 X. Sun, T. Zhao, J. Hu, Y. Bai, L. Meng, Q. Yang, Y. Zhou and W. Fu, *Sci. Total Environ.*, 2024, **917**, 170319.
56 N. Lai, W. Song, M. Wang, L. Zhao, J. Zhou, X. Cai, H. Fu, M. Zhang, Y. Sui, H. Sun, T. Song, Q. Sun and A. Li, *Processes*, 2024, **12**, 2713.
57 Y. Sun, C. Zhao, Y. Su, Z. Ma, J. Li, H. Letu, Y. Yang and H. Fan, *Earth Space Sci.*, 2019, **6**, 1915–1925.
58 Z. Xu, Z. Peng, N. Zhang, H. Liu, L. Lei and X. Kou, *Atmos. Environ.*, 2024, **318**, 120265.